Galvanomagnetic effects in semiconductors and semimentals

Peter Wagle

MASTER OF SCIENCE

GALVANOMAGNETIC EFFECTS

IN

SEMICONDUCTORS AND SEMIMETALS

by

PETER WAGLE B.Sc.

NOVEMBER, 1965.

CONTENTS.

Acknowledgements.

This thesis is submitted in fulfillment of the requirements for the degree of Master of Science of the University of Durham. The work has been supported in full by the Science Research Council (Department of Scientific and Industrial Research).

I am grateful to the staff of the Department of Applied Physics and in particular to Professor D.A. Wright who suggested the topic and directed my research and to Dr. C.J. Hearn with whom I have had many profitable discussions. Thanks are due to Mrs. J. Lincoln who typed the Thesis and to Miss E.J. Skinner who wrote the equations.

Introduction

This thesis is concerned with those aspects of the galvanothermomagnetic effects which are related to the performance of a semiconducting or semimettalic energy converter. Although the theory of isotropic galvanomagnetic devices can be developed relatively easily it is only recently (1963) that a full study of the refinements caused by crystal anisotropy has been completed.

An attempt is made here to present the elements necessary for an understanding of the problems involved in predicting the behaviour of an energy converter. A description of a refrigerator in a particular orientation is provided and serves to explain the physical principles underlying the operation of these devices.

Since there is available a great deal of experimental and theoretical information on graphite in single crystal or pyrolytic form and since graphite exhibits properties which suggest that it might behave efficiently as a refrigerator it has been chosen as a model.

The magnetic field dependent conductivity tensor is developed from what is known of the band structure and the Nernst coefficient is reduced to a simple form in terms of mobilities. These coefficients are applied to the figure of merit of the refrigeration device to give a numerical estimate of the efficiency of graphite as an energy converter.

Chapter 1 describes the Nernst-Ettingshausen refrigeration device operated in the transverse mode with the thermal gradient, electric

current and magnetic field mutually perpendicular. It is shown that the efficiency of the cooler depends on a figure of merit which is required to be as large as possible. The figure of merit is directly proportional, at a particular temperature, to the electrical conductivity, the thermal resistance and the Nernst coefficient. The material used in an efficient device should, therefore, have a high mobility and electrical conductivity and a low thermal conductivity.

The general equations of transport are developed in Chapter 2 and the galvanomagnetic coefficients are extracted from them in terms of a general scattering parameter. The assumption is made that the relaxation time of a carrier exhibits a power dependence on its energy.

The band structure of graphite is well documented and Chapter 3 merely serves as a brief resumé and as a source of references to the many contributions made to this topic.

Two types of scattering are thought to take place in graphite at temperatures in the range $0 < T < 300^{\circ}K$ and in Chapter 4 weak field expressions for the phenomenological coefficients are obtained for the cases of acoustic mode scattering and scattering on imperfections and crystallite boundaries.

The final Chapter discusses the saturation values of the conductivity tensor at high magnetic fields and concludes with numerical estimates of the figure of merit for graphite.

CHAPTER 1

The Nernst - Ettingshausen Refrigerator.

Energy conversion can be achieved with reasonable efficiency in semiconductor devices by making use of the thermoelectric or the galvanothermo-megnetic effects. The theory for the thermoelectric devices has been well established (1, 2) and the recent discussion (3, 4, 5, 6) of the Nernst - Ettingshausen power generators and refrigerators has developed in an analagous manner. The detailed analysis shows that the efficiency of the latter devices depends on an anisotropy factor and some clarity of the physical situation is lost in dealing with the anisotropic equations in the general approach. For this reason the isotropic Peltier refrigeration device is discussed briefly.

1.1 The Peltier Cooler.

Energy is emitted or absorbed when a current flows across the junction between a metal and an extrinsic semiconductor due to the discontinuity in average energy of the current carriers. Lattice vibrations provide the energy required when absorption takes place and there is a subsequent cooling of the material.

Temperature is re duced when the electric current flow is from n - type material to the metal and from the metal to p - type material. The device is shown in Fig. 1.1. The thermal reservoirs are at temperatures T_h and T_c, the junction resistance is supposed to be negligible and the electrical

resistance ρ , thermal conductivity K, and Seebech coefficient α are assumed to be independent of temperature.

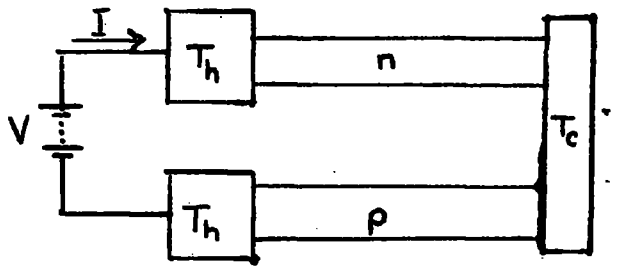

Fig. 1.1. The Peltier Cooler

The efficiency of the cooler is discussed in terms of the reduced coefficient of performance.

$$\phi_r = \frac{\phi}{\phi_c} = \phi \frac{\Delta T}{T_c} < 1 \qquad \ldots\ldots\ldots 1.1$$

where is the coefficient of performance defined as the ratio of the heat q_c , removed from the cooled reservoir devided by the electrical power input P.

$$\phi = \frac{q_c}{P} \qquad \ldots\ldots\ldots 1.2$$

ϕ_c is the maximum value of ϕ for a Carnot cycle

$$\phi_c = \frac{T_c}{\Delta T} \qquad \ldots\ldots\ldots 1.3$$

and

$$\Delta T = T_h - T_c > 0 \qquad \ldots\ldots\ldots 1.4$$

Joule heating in the sample caused by the flow of current together with thermal conduction from the hot reservoir cause an unwanted temperature rise at the cold junction. Thus the heat removal rate is reduced - from $\alpha T_c I$ - the rate of Peltier heat absorption - to

$$q_c = \alpha T_c I - \tfrac{1}{2} I^2 R - K\Delta T \qquad \text{.....1.5}$$

I is the electric current, K is the thermal conductance of the two arms in parallel and R is the resistance of the two arms in series.

$$K = \kappa_n \gamma_n + \kappa_p \gamma_p \qquad \text{.....1.6}$$

$$R = \frac{\rho_n}{\gamma_n} + \frac{\rho_p}{\gamma_p} \qquad \text{.....1.7}$$

where the subscripts n and p refer to each arm and γ_i, is the area to length ratio for each arm.

The applied voltage

$$V = \alpha \Delta T + IR \qquad \text{.....1.8}$$

so that the power imput

$$P = VI = \alpha I \Delta T + I^2 R \qquad \text{.....1.9}$$

Thus the coefficient of performance is

$$\phi = \frac{mT_c - \frac{1}{2}m^2 - \frac{KR}{\alpha^2}\Delta T}{m\Delta T + m^2} \qquad \text{.....1.10}$$

with $$m = \frac{IR}{\alpha}$$

ϕ may be optimised with respect to the ratio γ_n/γ_p by equating the derivative to zero.

Then

$$\left(\frac{\gamma_n}{\gamma_p}\right)_{opt} = \left(\frac{\kappa_p}{\kappa_n} \cdot \frac{\rho_n}{\rho_p}\right)^{1/2} \qquad \text{.....1.11}$$

and $$\phi_{opt} = \frac{mT_c - \frac{1}{2}m^2 - \frac{\Delta T}{Z}}{m\Delta T + m^2} \qquad \text{.....1.12}$$

where $$Z = \frac{\alpha^2}{\left[(\rho_n \kappa_n)^{1/2} + (\rho_p \kappa_p)^{1/2}\right]^2} \qquad \text{.....1.13}$$

$$= \frac{\alpha^2}{(KR)_{opt}}$$

is the figure of merit, requiring to be as large as possible.

The optimum coefficient of performance reaches a maximum value.

$$\phi_{max} = \frac{T_c}{\Delta T} \cdot \frac{\omega - T_h/T_c}{\omega + 1} \qquad \text{.....1.14}$$

when $$I = \frac{\alpha \Delta T}{R(\omega - 1)} \qquad \text{.....1.15}$$

and

$$\omega = (1 + Z\bar{T})^2 \qquad \text{.....1.16}$$

$$T = \frac{1}{2}(T_h + T_c) \qquad \text{.....1.17}$$

Finally the reduced coefficient of performance optimised for geometry and applied voltage

$$\phi_r = \frac{\omega - T_h/T_c}{\omega + 1} \qquad \text{.....1.18}$$

The maximum temperature difference, ΔT max., is found after setting

$$\phi_r = 0 \text{ to be } \quad \Delta T_{max} = \frac{1}{2} Z T_c^2 \qquad \text{.....1.19}$$

Delves (7) points out that a ZT_c of about unity must be optained for useful cooling at low temperatures requiring $Z \sim 10^{-2}$ at 80° K. Wolfe and Smith (8) have obtained $Z = 5 \times 10^{-3}$ (deg. C)$^{-1}$ at 80° K for an n - type Bi - Sb alloy, which is better than any of the values given by Heikes and Ure (1) but which is still rather low. A corresponding p - type material has yet to be found.

The search for a better figure of merit has caused attention to be turned to the thermogalvanomagnetic effects. The principal advantage is that only one material is required.

1.2 The Ettingshausen Effect.

In an extrinsic conductor the Ettingshausen effect (9, 10) is the production of a thermal gradient in the y - direction when a magnetic field preferentially deflects fast and slow current carriers flowing in the x - direction.

Near the intrinsic region both electrons and holes are deflected by the magnetic field to the same side where they recombine and release energy. On the opposite side generation takes place and energy is absorbed. This process provides and additional and often larger contribution than in the extrinsic case.

A rectangular configuration is supposed in the above description and the effect is formally described by

$$\frac{dT}{dy} = PH_z J_x \qquad \text{.....1.20}$$

where P is the Ettingshausen coefficient

1.3 The Nernst Effect.

The extrinsic Nernst effect (9) occurs when carriers diffusing along an applied temperature gradient are deflected by a magnetic field. The concentration of carriers produces a transverse electric field

$$E_y = QB_z \frac{dT}{dx} \qquad \text{.....1.21}$$

where Q is the Nernst coefficient.

1.4 The Galvano-thermomagnetic Refrigerator.

The theory for thermogalvanomagnetic generators and refrigerators has been treated extensively by Harman and Honig (5) and by Kooi et al. (6). The manner in which the Nernst and Ettingshausen coefficients enter the equations for the coefficient of performance is shown by particular reference to the transverse device.

For simplicity attention is restricted to the isothermal mode of operation although a subscript is not used on the various coefficients to specify the isothermal case.

Although Harman and Honig discuss a two arm device they show that no advantage is gained by using two different materials so that it is sufficient to examine the single rectangular bar configuration which is discussed by Kooi et al. (6) and treated rather less formally by numerous other authors, (3,4,5,7,9). The device is shown in Fig 1.2.

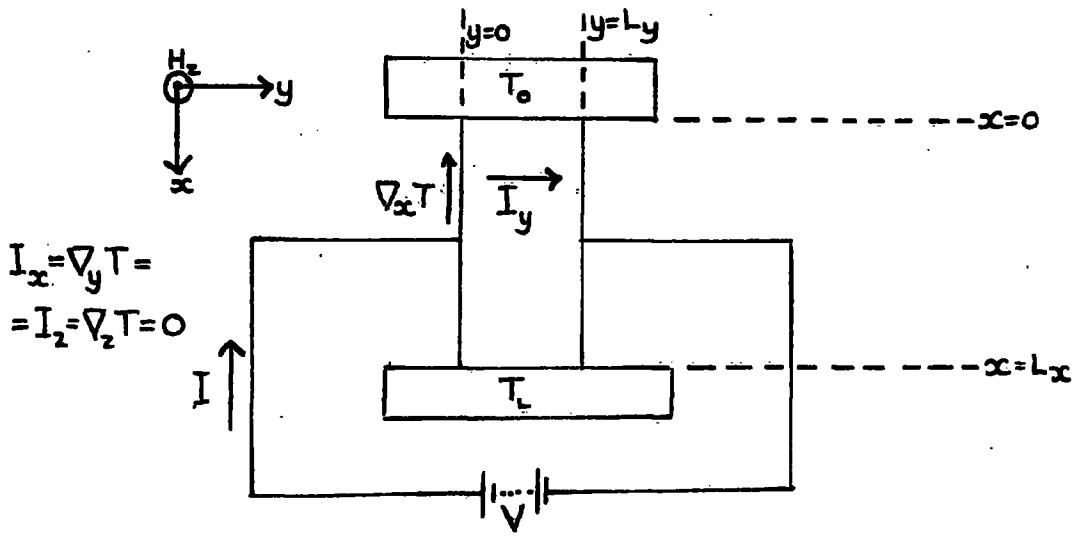

Fig. 1.2. The Nernst - Ettingshausen Refrigerator.

The rectangular parallelipiped bar is maintained between two heat resevoirs at temperatures T_o and T_L with $T_L > T_o$. The desired conventions and configuration are clearly shown in Fig 1.2. The magnetic field is $H = (0,0,H_z)$, $\underline{I} = (0,I_y,0)$ is the electric current and $\nabla_r T = (\nabla_x T, 0, 0)$ is the thermal gradient.

With these restrictions the phenomenological equations (5e,11) for an anisotropic material may be written in relatively simple form.

$$J_s^x = \frac{\kappa_{xx}}{T} \nabla_x T + (\alpha_{yx} - H_z Q_{yx}) J^y \qquad \ldots.1.22$$

$$J_s^y = \frac{-\kappa_{yx} + H_z \kappa_{yy} M_{yx}}{T} \nabla_x T + (\alpha_{yy} - H_z Q_{yy}) J^y \qquad \ldots..1.23$$

$$\nabla_x V^* = (\alpha_{xx} + H_z Q_{xx}) \nabla_x T + (\rho_{yx} - H_z R_{yx}) J^y \qquad \ldots..1.24$$

$$\nabla_y V^* = (\alpha_{yx} + H_z Q_{yx}) \nabla_x T + \rho_{yy} J^y \qquad \ldots...1.25$$

$\underline{E} = -\nabla_r (V)$ is the electric field, $V^* = -\frac{\zeta}{se} + V$ $s = \pm 1$ according as the material is p or n type and ζ is the Fermi enefgy.

The entropy flux density is J_s and the electric current density is $\underline{J}$.

$\rho_{ij}, Q_{ij}, R_{ij}, \alpha_{ij}, K_{ij}$ and L_{ij} are the resistivity, Nernst coefficient, Hall coefficient, Seebeck coefficient, thermal conductivity and Righi-Leduc coefficient respectively.

A differential equation for the temperature distribution T_x along the bar is obtained by Harman & Honig (5e) with the assumption that the current I_y is constant. Their claim that the error involved is not large is validated in a short discussion by Honig & Tammy (12) and by the fact that, although an approximation is obtained for the temperature distribution, the resultant expression for the coefficient of performance and maximum temperature difference is equivalent to that obtained by Kooi (et al.)(6).

It will, therefore, be assumed that Iy is a constant. As energy is conserved in the system the equation of continuity applied to the total energy vector $\underline{J}_\varepsilon$ is (13)

$$\operatorname{div} \underline{J}_\varepsilon = 0 \qquad \text{.....1.26}$$

with $$\underline{J}_\varepsilon = T\underline{J}_s - \psi \underline{J} \qquad \text{.....1.27}$$

giving $$\nabla_x (T J_s^x) + \nabla_y (T J_s^y - \psi J^y) = 0 \qquad \text{.....1.28}$$

since $$J^x = 0$$

Substituting for J_s^x , J_s^y and $\nabla_y \psi$ from equations 1.22 1.23 and 1.24 and assuming that each transport coefficient is replaced by its average value denoted by a bar gives a second order linear differential equation for the temperature distribution.

$$\bar{K}_{xx} \nabla_x^2 T + 2H_z \bar{Q}_{yx} \bar{J}^y \nabla_x T + \bar{\rho}_{yy} (\bar{J}_y)^2 = 0 \quad \ldots\ldots 1.29$$

Kooi (et alia)(6) treat the case when the Nernst coefficient and the resisitivity are proportional to T^{-1} and obtain the same coefficiant of performance. Equation 1.29 is solved approximately if T(x) can be expanded as a Taylor series about its value at x = o

$$T(x) = T(0) + xT'(0) + \frac{x^2}{2} T''(0) \quad \ldots.1.30$$

Retaining powers of x up to x^2 and using the boundary conditions

$$T_\delta = T_{x=0}, \; T_L = T_{x=L_x} \quad \ldots.1.31$$

gives $$T(0) = \frac{\Delta T}{L_x} + \left(b + a \frac{\Delta T}{L_x}\right) \frac{L_x}{2} \quad \ldots.1.32$$

where $$a = \frac{2H_z \bar{Q}_{yx} \bar{J}^y}{\bar{K}_{xx}} \quad \ldots.1.33$$

$$b = \frac{\rho_{yy} (\bar{J}^y)^2}{\bar{K}_{xx}} \quad \ldots.1.34$$

and $$\Delta T = T_L - T_o > 0 \qquad \text{.....1.35}$$

The sample has sides of length L_λ (λ = x,y,z) and cross - sectional area A_λ perpendicular to the direction λ .

The coefficient of performance C of the device is the ratio of the rate of transfer of energy to the cold reservoir, $\dot{\mathcal{E}}_{x=o}$, to the power imput, P, to the device

$$C = \frac{\dot{\mathcal{E}}_{x=o}}{P} \qquad \text{.....1.36}$$

The total energy flux past the junction at

$$\dot{\mathcal{E}}_{x=o} = A_x J_\varepsilon^x \qquad \text{.....1.37}$$

Substituting for J_ε^x from equations 1.27 and 1.22 and neglecting the junction resistance term involving $\psi_{x=o}$

gives $$\dot{\mathcal{E}}_{x=o} = -\bar{\kappa}_{xx} A_x \frac{\Delta T}{L_x} - \left(\bar{b} + \bar{a}\frac{\Delta T}{L_x}\right)\frac{L_x}{2} A_x + \qquad \text{.....1.38}$$

$$+ T_o\left(\bar{\alpha}_{yx} - H_z \bar{Q}_{yx}\right) A_x \bar{J}_x^y$$

Since the total current is $I_y = A_y J^y$ 1.39

expression 1.38 may be abreviated to

$$\dot{\varepsilon}_{x=0} = -\bar{K}_{xx}\Delta T - \tfrac{1}{2}\bar{R}_{yy}\bar{I}_y^2 + \qquad \text{.....1.40}$$

$$+ I_y\left[\bar{T}\left(\bar{A}_{yx} - H_z\bar{N}_{yx}\right) - \tfrac{1}{2}\Delta T\left(\bar{A}_{yx} + H_z\bar{N}_{yx}\right)\right]$$

$$\bar{K}_{xx} = \bar{\kappa}_{xx}\frac{A_x}{L_x} \qquad \text{.....1.41}$$

$$\bar{R}_{yy} = \bar{\rho}_{yy}\frac{L_y}{A_y} \qquad \text{.....1.42}$$

$$\bar{A}_{yx} = \bar{\alpha}_{yx}\frac{L_y}{L_x} \qquad \text{.....1.43}$$

$$\bar{N}_{yx} = \bar{Q}_{yx}\frac{L_y}{L_x} \qquad \text{.....1.44}$$

$$\text{and } \bar{T} = \tfrac{1}{2}\left(T_L + T_o\right) \qquad \text{.....1.45}$$

The electric current, Iy, is determined by evaluating the line integral of $\nabla_y\psi$ round the circuit.

Thus. $V = \Delta T\left[\bar{A}_{yx} + H_z\bar{N}_{yx}\right] + \bar{R}_{yy}\bar{I}_y$ ...1.46

Where V is the applied electromotive force.

The electrical power imput is then

$$P = VI_y = \Delta T[\bar{A}_{yx} + H_z\bar{N}_{yx}]\bar{I}_y + \bar{R}_{yy}\bar{I}_y^2 \qquad \ldots.1.47$$

and the coefficient of performance (equ.1.36) is

$$C = -\frac{\bar{K}_{xx}\Delta T + \frac{1}{2}\bar{R}_{yy}\bar{I}_y^2 + \bar{I}_y[\bar{T}(H_z\bar{N}_{yx} - \bar{A}_{yx}) + \frac{1}{2}\Delta T(\bar{A}_{yx} + H_z\bar{N}_{yx})]}{\Delta T[\bar{A}_{yx} + H_z\bar{N}_{yx}]\bar{I}_y + \bar{R}_{yy}\bar{I}_y^2} \qquad \ldots.1.48$$

The optimum value, C^*, is obtained by equating the derivative $\frac{\partial C}{\partial \bar{I}_y}$ to zero.

Then the optimum value of the current is

$$I_y^* = -\bar{K}_{xx}\frac{\Delta_x T}{\bar{T}}\frac{(1+\delta_y)}{H_z\bar{N}_{yx} - \bar{A}_{yx}} \qquad \ldots.1.49$$

where $$\delta_y = (1 + Y\bar{T})^{1/2} \qquad \ldots.1.50$$

$$Y = r_{yx}Z \qquad \ldots.1.51$$

$$Z = \frac{(\bar{A}_{yx} + H_z\bar{N}_{yx})}{\bar{K}_{xx}\bar{R}_{yy}} \qquad \ldots.1.52$$

and $$r_{yx} = \frac{H_z \bar{N}_{yx} - \bar{A}_{yx}}{H_z \bar{N}_{yx} + \bar{A}_{yx}} \qquad \ldots\ldots 1.53$$

Substituting I_y^* into equation 1.48 gives

$$C^* = \frac{T_o}{\Delta T}\left[\frac{r_{yx}\cdot\frac{\bar{T}}{T_o}(1+\delta_y) - \frac{\Delta T}{2T_o}(1+\delta_y)}{1+\delta_y}\right] \qquad \ldots\ldots 1.54$$

The maximum temperature difference is found by optimising $\dot{\varepsilon}_{x=0}$ (equ.1.40) for I_y and equating to zero when

$$(\Delta T)_{max} = \tfrac{1}{2}\bar{T}^2 r_{yx} Y \qquad \ldots\ldots 1.55$$

When α_{yx} is small, r_{yx} tends to unity and Y tends to

$$Z_\varepsilon \doteq \frac{(H_z \bar{Q}_{yx})^2}{\bar{\kappa}_{xx}\bar{\rho}_{yy}} \qquad \ldots\ldots 1.56$$

Then the maximum temperature difference is

$$(\Delta T)_{max} = \tfrac{1}{2} Z_\varepsilon \bar{T}^2 \qquad \ldots\ldots 1.57$$

and Z_ε is seen to be the figure of merit for the Nernst-Ettingshausen device. Suitable orientation of the crystal provides an optimum value.

The criteria for a large value for Z_e are a high Nernst coefficient and electrical conductivity and a low thermal conductivity.

The expression 1.56 is obtained (6) if the crystal used in the device can be orientated so that the various fluxes are directed along principal axes which are mutually perpendicular.

CHAPTER 2

The transport equations and the galvanomagnetic coefficients.

Magnetic field dependant expressions are obtained for the galvanomagnetic tensors which are coefficients in relations between electric and heat current densities and applied electrochemical fields and thermal gradients. The tensor components are obtained in terms of the solution of the Boltzmann equation assuming the existance of a relaxation time for some particular cases. Further assuming that the relaxation time τ has a power dependence on energy ($\tau = b\epsilon^{\lambda}$) an expression is given for the Nernst coefficient in an anisotropic conductor with arbitrary scattering parameter, λ in terms of partial mobilities, Fermi levels and Fermi integrals.

2.1 The Transport Equations.

The phenomenological equations relating current density flow to applied electric, magnetic and thermal fields are established by the theory of irreversible processes (13, 14, 15, 16) to be of the form

$$J_i = \sigma_{ij}(\underline{H}) E_j^* + M_{ij}(\underline{H}) \frac{\partial T}{\partial x_j} \qquad \ldots\ldots 2.1$$

$$q_i = N_{ij}(H) E_j^* + L_{ij}(\underline{H}) \frac{\partial T}{\partial x_j} \qquad \ldots\ldots 2.2$$

where $$E_j^* = E_j + \frac{1}{e}\frac{\partial \zeta}{\partial x_j} = \frac{1}{e}\frac{\partial V}{\partial x_j} \qquad \ldots\ldots 2.3$$

is the electrochemical field

E_j and $\frac{\partial T}{\partial x_j}$, are respectively the cartesiun components of electric field and thermal gradient.

$\underline{J}$ and $\underline{q}$ are electric and thermal current densities

V is the electrochemical potential

and - e is the electronic charge.

A summation convention is used over repeated indices.

When more than one type of carrier is present the total current density is obtained by summation over contributions due to individual carriers.

The choice of grad V and grad T as forces and $\left[1/(-e)\right] \underline{J}$ and $\left[1/T\right] \underline{q}$ as mass and entropy flows permits the application (16) of the Onsager relations.

Thus $$\sigma_{ij}(\underline{H}) = \sigma_{ji}(-\underline{H}) \qquad \ldots\ldots 2.4$$

$$L_{ij}(\underline{H}) = L_{ji}(-\underline{H}) \qquad \ldots\ldots 2.5$$

$$N_{ij}(\underline{H}) = -TM_{ij}(-\underline{H}) \qquad \ldots\ldots 2.6$$

σ is the electrical conductivity defined as the reciprocal to the resistivity tensor ρ. The other coefficients M, N and L are not easily observable but can be expressed in terms of more familiar effects by inversion of equations (2.1) and (2.2)

$$E_i^* = \rho_{ik}(\underline{H})\, J_k + \alpha_{ik}(\underline{H}) \frac{\partial T}{\partial x_j} \qquad \ldots\ldots\ldots 2.7$$

$$q_i = \pi_{ik}(\underline{H}) J_k - \kappa_{ik}(\underline{H}) \frac{\partial T}{\partial x_j} \qquad \ldots\ldots\ldots 2.8$$

where

$$\rho_{ij}\, \sigma_{jk} = \delta_{ik} \qquad \ldots\ldots\ldots 2.9$$

$$\alpha_{ik} = \rho_{ik} M_{jk} \qquad \ldots\ldots\ldots 2.10$$

$$\pi_{ik} = N_{ij}\, \rho_{jk} \qquad \ldots\ldots\ldots 2.11$$

$$\kappa_{ik} = N_{ij}\, \rho_{jl} M_{lk} - L_{ik} \qquad \ldots\ldots\ldots 2.12$$

and

$$\rho_{ik}(\underline{H}) = \rho_{ki}(-\underline{H}) \qquad \ldots\ldots\ldots 2.13$$

$$\kappa_{ik}(\underline{H}) = \kappa_{ki}(-\underline{H}) \qquad \ldots\ldots\ldots 2.14$$

$$\pi_{ik}(\underline{H}) = T \alpha_{ki}(-\underline{H}) \qquad \ldots\ldots\ldots 2.15$$

α is the absolute thermoelectric power, π is the absolute Peltier coefficient and κ is the thermal conductivity.

2.2 The Galvanomagnetic Coefficients.

Expressions for the transport coefficients are obtained by considering the distribution function $f(\underline{k},\underline{r})$ of the charge carriers under the influence of applied fields. $f(\underline{k},\underline{r})$ is the probability that a carrier exists in a state with wave vector $\underline{k}$ and position vector $\underline{r}$. With this definition the number of charge carriers in a volume element with wave vectors $\underline{k}$ in the element $d^3\underline{k}$ is $\frac{1}{4\pi^3} f(\underline{k},\underline{r})\, d^3\underline{k}\, d^3\underline{r}$

In the absence of fields the carriers obey Fermi-Dirac statistics (17) and

$$f \equiv f_o = \frac{1}{1+\exp\left(\frac{\epsilon-\zeta}{kT}\right)} \qquad \text{.....2.16}$$

where ϵ is energy, ζ is the Fermi level and T is the absolute temperature. k is Boltzman's constant.

Knowledge of the distribution function gives an explicit form for the current density equations (18).

$$\underline{J} = -\frac{e}{4\pi^3} \int \underline{v} f \, d^3\underline{k} \qquad \text{.....2.17}$$

$$\underline{q}_{el} = \frac{1}{4\pi^3} \int \underline{v} (\epsilon - \zeta) f \, d^3\underline{k} \qquad \text{.....2.18}$$

$\underline{v}$ is the carrier velocity. The subscript el indicates that only the electronic contribution to the heat current density is given by equation (2.18).

The distribution function arises as the solution of the Boltymann integro-differential equation. A derivation is indicated in Appendix 2.A. The equation is

$$-\frac{e}{\hbar}\left(\underline{E}+\frac{1}{c}\underline{v}\wedge\underline{H}\right)\cdot\nabla_k f+\underline{v}\cdot\nabla_r f=\left(\frac{\partial f}{\partial t}\right)_{coll} \qquad \text{.....2.19}$$

where $\underline{E}$ is the electric field, $\underline{H}$ is the magnetic field and ∇ is the gradient operator.

The term $\left(\frac{\partial f}{\partial t}\right)_{coll}$ represents the contribution to changes in the distribution function caused by collisions of charge carriers with lattice imperfections. This change may be represented as a collision integral (7)

$$\left(\frac{\partial f}{\partial T}\right)_{coll}=\int\left\{S(\underline{k}',\underline{k})f(\underline{k}')[1-f(\underline{k})]-S(\underline{k},\underline{k}')f(\underline{k})[1-f(\underline{k}')]\right\}d\underline{k}' \qquad \text{.....2.20}$$

in which a carrier is taken by a collision from the state $\underline{k}$ to the state and $S(\underline{k},\underline{k}')$ is the probability per unit time interval that the carrier makes the transition.

$f(k_i)[1-f(k_f)]$ is the probability that the state k_i is occupied and the state k_f is unoccupied.

The solution of equation 2.19 with $\left(\frac{\partial f}{\partial t}\right)_{coll}$ given by equation 2.20 can be obtained by variational methods (20) but it is usual to assume that a relaxation time τ governs the approach of the distribution function to its equilibrium value after the external fields have been removed and

under the influence only of collisions of carriers with lattice imperfections. That is

$$(f-f_o)_t = (f-f_o)_{t=0} \exp(-t/\tau) \qquad \text{.....2.21}$$

or

$$\left(\frac{\partial f}{\partial t}\right)_{coll} = -\frac{f-f_o}{\tau} \qquad \text{.....2.22}$$

The existence of a relaxation time is discussed by Beer (16) who points out that the assumption is justified for elemental semiconductors provided that the energy emitted or absorbed by a carrier at collision is small compared with its initial velocity (21, 22, 23)

With the collision term represented by equations 2.22, Boltzmann's equation reduces to a first order linear differential equation.

$$-\frac{e}{\hbar}\left[\underline{E}+\frac{1}{c}\underline{v}\wedge\underline{H}\right]\cdot\nabla_k f+\underline{v}\cdot\nabla_r f=-\frac{f-f_o}{\tau} \qquad \text{.....2.23}$$

which can be solved by letting

$$f=f_o-\Phi(\underline{k})\frac{\partial f_o}{\partial \epsilon} \qquad \text{.....2.24}$$

substituting

$$\underline{v}=\frac{1}{\hbar}\nabla_k \epsilon \qquad \text{.....2.25}$$

and retaining first order terms.

This results in an equation for ϕ

$$\frac{e}{\hbar}\underline{F}\cdot\nabla_k\epsilon+\frac{e}{\hbar^2c}\underline{H}\cdot\Omega\phi=-\frac{\phi}{\tau} \qquad \text{.....2.26}$$

where $$\Omega=\nabla_k\epsilon\cdot\nabla_k \qquad \text{.....2.27}$$

$$=\epsilon_{ijl}\frac{\partial\epsilon}{\partial k_j}\frac{\partial}{\partial k_l} \qquad \text{.....2.28}$$

where ϵ_{ijl} is the permutation tensor

$$\left.\begin{aligned}&\epsilon_{123}=\epsilon_{312}=\epsilon_{231}=1\\&\epsilon_{321}=\epsilon_{132}=\epsilon_{213}=-1\\&\text{other components zero}\end{aligned}\right\} \qquad \text{.....2.29}$$

$\underline{F}=\underline{E}-\frac{T}{e}\nabla_r\left(\frac{e-\zeta}{T}\right)$ is the applied electrothermal field.

Equation 2.26 is solved by an iteration process (24). To zero order in magnetic field.

$$\phi^0=-\frac{e\tau}{\hbar}\underline{F}\cdot\nabla_k\epsilon \qquad \text{.....2.30}$$

Substitution in the second term of equation 2.26 gives

$$\phi'=-\frac{e\tau}{\hbar}\left\{\underline{F}\cdot\nabla_k\epsilon-\frac{e}{\hbar^2c}\underline{H}\cdot\Omega\left(\tau\underline{F}\cdot\nabla_k\epsilon\right)\right\} \qquad \text{.....2.31}$$

ans so on, for a series expansion for ϕ in rising powers of the magnetic field

$$\phi = -\frac{eT}{\hbar}\left\{\underline{F}\cdot\nabla_k\epsilon - \frac{e}{\hbar^2 c}\underline{H}\cdot\Omega(T\underline{F}\cdot\nabla_k\epsilon) + \right.$$
$$\left. + \left(\frac{e}{\hbar^2 c}\right)^2 \underline{H}\cdot\Omega\{T\underline{H}\cdot\Omega(T\underline{F}\cdot\nabla_k\epsilon)\} + \ldots\right\} \quad \ldots\ldots 2.32$$

The approach must evidently be used when the magnetic field is small enough to allow reasonable convergence of the series. In addition the expansion and the Boltzmann equation itself is subject to the quantum limit

$$\frac{eTH}{m^* c} < 1 \quad \ldots\ldots 2.33$$

The procedure for high magnetic fields below $\frac{m^* c}{eT}$ is discussed by Shockley (25, 26, 27) and others and quantum effects are discussed by Beer (16). It is assumed here that the inequality 2.33 applies.

The substitution of equation 2.24 in equations 2.17 and 2.18 gives

$$\underline{J} = \frac{e}{4\pi^3\hbar}\int \nabla_k\epsilon\,\phi\,\frac{\partial f_o}{\partial\epsilon}\,d^3\underline{k} \quad \ldots\ldots 2.34$$

$$\underline{q}_{el} = -\frac{1}{4\pi^3\hbar}\int \nabla_k\epsilon(\epsilon-\zeta)\phi\,\frac{\partial f_o}{\partial\epsilon}\,d^3\underline{k} \quad \ldots\ldots 2.35$$

since there is no current contribution due to the equilibrium terms involving f_o .

Expression 2.32 for ϕ , when used in equations 2.34 and 2.35 gives explicit if cumbersome expressions for the galvanomagnetic coefficients after reduction to the form of equations 2.1 and 2.2. More useful expressions are obtained by examining some particular cases.

2.3 Quadratic Energy Surfaces.

When the carrier energy is a quadratic function of $\underline{k}$ the Boltzmann equation can be solved exactly. With a suitable choice of co-ordinates it is possible to write

$$\epsilon(\underline{k}) = \frac{1}{2}\hbar^2 \left[\frac{k_1^2}{m_1} + \frac{k_2^2}{m_2} + \frac{k_3^2}{m_3}\right] \qquad \ldots\ldots 2.36$$

The thermogalvanomagnetic effects in many conductors can be predicted using an arrangement of such ellipsoids in accordance with the symmetry of the crystals (28, 29) it is found that usually $m_1 = m_2 = m_\perp$, $m_3 = m_\parallel$. where $\perp$ and $\parallel$ indicate directions perpendicular and parallel to the long axis of the ellipsoid.

As an ellipsoid can be reduced to a sphere using a linear transformation it is useful to study the isotropic effects and to deduce the general quadratic case. The results will have the same form (30) except that σ^2 terms will be replaced by $\sigma_\parallel \sigma_\perp$.

With energy given by 2.36 ϕ may be written in closed form.

$$\phi = -\frac{e\tau}{\hbar}\nabla_k \epsilon \cdot \frac{\left\{\underline{F} - \frac{\tau e}{c}\left(\frac{\underline{F}}{m}\right)\wedge \underline{H} + \left(\frac{\tau e}{c}\right)^2 \frac{(\underline{F}\cdot\underline{H})(m\underline{H})}{|m|}\right\}}{1 + \left(\frac{\tau e}{c}\right)^2 \frac{(m\underline{H}\cdot\underline{H})}{|m|}}$$

$\ldots\ldots 2.37$

where m and $|m|$ are the effective mass tensor and its determinant.

2.4 The Transport Equations in an Isotropic Medium.

In an isotropic medium the ellipsoids of the previous section are reduced to spheres and

$$\epsilon = \frac{\hbar^2}{2} \frac{k^2}{m} \qquad \ldots\ldots\ldots 2.38$$

is parabolic in $\underline{k}$ - space

The expression for Φ simplifies to

$$\Phi = -\frac{e\tau}{\hbar} \nabla_k \epsilon \cdot \frac{\left\{\underline{F} - \left(\frac{e\tau}{mc}\right)\underline{F} \wedge \underline{H} + \left(\frac{e\tau}{mc}\right)^2 (\underline{F}\cdot\underline{H})\underline{H}\right\}}{1 + \left(\frac{e\tau}{mc}\right)^2 H^2} \qquad \ldots\ldots\ldots 2.39$$

since the effective mass tensor reduces to the scaler m.

Expressions for the transport coefficients are obtained (31) by expressing Φ and equations 2.34 and 2.35 in tensor form and comparing with equations 2.1 and 2.2.

For a cartesian coordinate system with

$$\sigma_{xx} = \sigma_{yy} = C_1 \qquad \ldots\ldots\ldots 2.40$$

$$\sigma_{xy} = -\sigma_{yx} = -D_1 \qquad \ldots\ldots\ldots 2.41$$

$$\sigma_{xz} = \sigma_{yx} = -\sigma_{zx} = -\sigma_{zy} = 0 \qquad \ldots\ldots\ldots 2.42$$

$$\sigma_{zz}(\underline{H}) = \sigma_{xx}(0) \qquad \ldots\ldots\ldots 2.43$$

$$M^{el}_{xx} = \frac{1}{e\tau}\left[C_2 - \zeta C_1\right], \quad M^{el}_{xy} = -\frac{1}{e\tau}\left[D_2 - \zeta D_1\right] \qquad \ldots\ldots\ldots 2.44$$

$$N_{xx}^{el} = -\frac{1}{e}\left[C_2 - \zeta C_1\right], \quad N_{xy}^{el} = \frac{1}{e}\left[D_2 - \zeta D_1\right] \qquad \ldots\ldots.2.45$$

$$L_{xx}^{el} = -\frac{1}{e^2T}\left[C_3 - 2\zeta C_2 + \zeta^2 C_1\right] \qquad \ldots\ldots.2,46$$

$$L_{xy}^{el} = \frac{1}{e^2T}\left[D_3 - 2\zeta D_2 + \zeta^2 D_1\right] \qquad \ldots\ldots.2.47$$

Tye symmetry relations expressed in equations 2.41 and 2.42 apply to the other coefficients.

$$C_n = -\frac{2e^2(2m)^{1/2}}{3\pi^2\hbar^3}\int_0^\infty \frac{T}{1+(\omega T)^2}\,\epsilon^{n+1/2}\,\frac{\partial f_o}{\partial \epsilon}\,d\epsilon \qquad \ldots\ldots.2.48$$

$$D_n = -\frac{2e^2(2m)^{1/2}}{3\pi^2\hbar^3}\int_0^\infty \frac{\omega T^2}{1+(\omega T)^2}\,\epsilon^{n+1/2}\,\frac{\partial f_o}{\partial \epsilon}\,d\epsilon \qquad \ldots\ldots.2.49$$

$$\omega = \frac{eH}{mc}, \quad e > 0 \text{ for electrons}$$

The equations 2.1 and 2.2 may be inverted so that the conductivity, Hall coefficient, Nernst coefficient and thermoelectric power can be expressed simply.

Equation 2.1 becomes (32).

$$\frac{\partial V^*}{\partial x} = A_{11} i_x + A_{12} i_y - A_{13} \frac{\partial}{\partial x}\left(\frac{1}{kT}\right) - A_{14} \frac{\partial}{\partial y}\left(\frac{1}{kT}\right) \qquad \text{.....2.50}$$

$$\frac{\partial V^*}{\partial y} = -A_{12} i_x + A_{11} i_y + A_{14} \frac{\partial}{\partial x}\left(\frac{1}{kT}\right) - A_{13} \frac{\partial}{\partial y}\left(\frac{1}{kT}\right) \qquad \text{.....2.51}$$

$$V^* = (\zeta - e\Theta)/kT = V/kT \qquad \text{.....2.52}$$

$$\underline{E}^* = \frac{1}{e} \nabla_r V \qquad \text{.....2.53}$$

Θ is an electrostatic potential associated with

$$J_i = -e i_i, \; e > 0 \text{ for electrons} \qquad \text{.....2.54}$$

$$A_{11} = \frac{3m}{2kT} \frac{K_1}{K_1^2 + H_1^2} \qquad \text{.....2.55}$$

$$A_{12} = \frac{3m}{2kT} \frac{H_1}{K_1^2 + H_1^2} \qquad \text{.....2.56}$$

$$A_{13} = -\left\{ \frac{K_1 K_2 + H_1 H_2}{K_1^2 + H_1^2} - e\Theta \right\} \qquad \text{.....2.57}$$

$$A_{14} = \frac{K_1 H_2 - H_1 K_2}{K_1^2 + H_1^2} \qquad \text{.....2.58}$$

$$K_n = -\frac{3m}{2e^2} C_n \qquad \text{.....2.59}$$

$$H_n = -\frac{3m}{2e^2} D_n \qquad \text{.....2.60}$$

2.5 Isothermal Effects.

The electrical conductivity

$$\sigma = J_x / E_x \text{ with } \frac{dT}{dx} = \frac{dT}{dy} = J_y = 0 \qquad \text{.....2.61}$$

$$\sigma = -\frac{e^2}{kT} \frac{1}{A_{11}}$$

The Hall coefficient.

$$R = \frac{E_y}{J_x H} \text{ with } \frac{dT}{dx} = \frac{dT}{dy} = J_y = 0 \qquad \text{.....2.62}$$

$$R = \frac{kT}{e^2 H} A_{12}$$

The Nernst coefficient.

$$Q = \frac{E_y}{H(-dT/dx)} \text{ with } J_x = J_y = \frac{dT}{dy} = 0 \qquad \text{...2.63}$$

$$Q = \frac{1}{TeH} A_{14}$$

The Thermoelectric Power

$$\alpha = \frac{E_x}{dT/dx} \quad \text{with} \quad J_x = J_y = \frac{dT}{dy} = 0 \qquad \ldots\ldots 2.64$$

$$\alpha = \frac{k}{e}\left\{\frac{A_{13}}{kT} + V^*\right\}$$

2.6 Mixed Conduction.

The equations used so far apply when only one type of carrier is present. When two carriers take part in conduction, the contribution to the current of each band is evaluated individually with the correct sign for the carrier charge and the total current is obtained by summation. For an isotropic medium the valence band energy is

$$\mathcal{E} = -E_g - \frac{\hbar^2}{2}\frac{|k|^2}{m_2} \qquad \ldots\ldots 2.65$$

where E_g is the energy gap between bands.

$E_g > 0$ for semiconductors and energies are referred to the bottom of the conduction band.

The Fermi levels for electrons and holes are related by $E_g = -(\zeta_1 + \zeta_2)$, where the subscripts 1 and 2 refer to electrons and holes respectively. The summation for the two carrier case has been carried out by Putley (32) and his results are quoted for the isotropic, isothermal case.

$$\sigma = \frac{(\sigma_1+\sigma_2)^2 + H^2\sigma_1^2\sigma_2^2(R_1+R_2)^2}{\sigma_1[1+H^2R_2^2\sigma_2^2]+\sigma_2[1+H^2R_1^2\sigma_1^2]} \qquad \ldots\ldots 2.66$$

$$R = \frac{R_1\sigma_1^2 + R_2\sigma_2^2 + H^2\sigma_1^2\sigma_2^2 R_1R_2(R_1+R_2)}{(\sigma_1+\sigma_2)^2 + H_2\sigma_1^2\sigma_2^2(R_1+R_2)^2} \qquad \ldots\ldots 2.67$$

$$Q = [Q_1\{\sigma_1(\sigma_1+\sigma_2)+\sigma_1^2\sigma_1^2 R_2(R_1+R_2)H^2\}+Q_2\{\sigma_2(\sigma_1+\sigma_2)+\sigma_1^2\sigma_2^2 R_1(R_1+R_2)H^2\}+$$
$$+\sigma_1\sigma_2(\alpha_1-\alpha_2)(R_1\sigma_1-R_2\sigma_2)]\times \qquad \ldots\ldots 2.68$$
$$\times[(\sigma_1+\sigma_2)^2+H^2\sigma_1^2\sigma_2^2(R_1+R_2)^2]^{-1}$$

$$\alpha = [\alpha_1\{\sigma_1(\sigma_1+\sigma_2)+\sigma_1^2\sigma_1^2 R_2(R_1+R_2)H^2\}+\alpha_2\{\sigma_2(\sigma_1+\sigma_2)+\sigma_1^2\sigma_2^2 R(R_1+R_2)H^2]-$$
$$-\sigma_1\sigma_2(Q_1-Q_2)(R_1\sigma_1-R_2\sigma_2)H^2]\times \qquad \ldots\ldots 2.69$$
$$\times[(\sigma_1+\sigma_2)^2+H^2\sigma_1^2\sigma_2^2(R_1+R_2)^2]^{-1}$$

2.7 The Single Ellipsoidal Energy Surface.

The expressions for Q (equation 2.68) may be extended (33) to cover the case of a single ellipsoidal energy surface. Then

$$Q_{yx} = \frac{Q_{yx}(n)\sigma_x(n)+Q_{yx}(p)\sigma_x(p)}{\sigma_x(n)+\sigma_x(p)} +$$
$$+\frac{[R_{yx}(n)\sigma_x(n)-R_{yx}(p)\sigma_x(p)]\sigma_y(n)\sigma_y(p)(\alpha_n-\alpha_p)}{[\sigma_x(n)+\sigma_x(p)][\sigma_y(n)+\sigma_y(p)]} \qquad \ldots\ldots 2.70$$

n and p refer to electrons and holes respectively

x is the direction of the electric field

y is the direction of the thermal gradient

and $\underline{H}$ is in the z - direction.

It will be shown later that Q, R and σ are related for each band if the relaxation time can be represented as a power of the energy.

$$\tau = b e^{\lambda} \qquad \ldots.2.71$$

Then $$Q_i = \pm \lambda \frac{k}{e} a_i R_i \sigma_i \qquad \ldots..2.72$$

i = 1 or 2 and the negative or positive sign are used for electrons or holes respectively and $e > 0$, σ_{ii} has been abbreviated to σ_i

When the substitution for Q_i is made.

$$Q_{yx} = \frac{\lambda k}{e} \left\{ \frac{-a_n R_{yx}(n)\sigma_y(n)\sigma_x(n) + a_p R_{yx}(p)\sigma_x(p)\sigma_y(p)}{\sigma_x(n)+\sigma_x(p)} \right.$$
$$\left. + \frac{[R_{yx}(n)\sigma_x(n) - R_{yx}(p)\sigma_x(p)]\sigma_y(n)\sigma_y(p)(\alpha_n - \alpha_p)}{[\sigma_x(n)+\sigma_x(p)][\sigma_y(n)+\sigma_y(p)]} \right\} \qquad \ldots..2.73$$

2.8 General Energy Surfaces.

Expressions can be obtained for the isothermal electrical conductivity and Hall coefficient when the energy is an arbitrary function of wave vector.

The electrical conductivity tensor $\sigma_{ij}(\underline{H})$ is expanded as a power series in $\underline{H}$ about its zero field value

$$J_i = \sigma_{ij}(\underline{H})\, E_j \qquad \ldots.2.74$$

and $$\sigma_{ij}(\underline{H}) = \sigma_{ij}^{\circ} + \sigma_{ijl}^{\circ} H_l + \sigma_{ijlm}^{\circ} H_l H_m + \ldots \qquad \ldots.2.75$$

with $$\sigma_{ijl}^{\circ} = \left(\frac{\partial \sigma_{ij}(\underline{H})}{\partial H_l} \right)_{\underline{H}=0} \qquad \ldots.2.76$$

$$\sigma_{ijlm}^{\circ} = \left(\frac{\partial^2 \sigma_{ij}(\underline{H})}{\partial H_l \partial H_m} \right)_{H=0} \qquad \ldots.2.77$$

and $\omega\tau < 1$.

Substitution of Φ (equation 2.32) into 2.34 gives (34)

$$\sigma_{ij}^{\circ} = -\frac{e^2}{4\pi^3 \hbar^2} \int \tau \frac{\partial f_o}{\partial \epsilon} \frac{\partial \epsilon}{\partial k_i} \frac{\partial \epsilon}{\partial k_j} d^3k \qquad \ldots.2.78$$

$$\sigma_{ijl}^{\circ} = +\frac{e^3}{4\pi^3 \hbar^4 c} \int \tau \frac{\partial f_o}{\partial \epsilon} \frac{\partial \epsilon}{\partial k_i} \frac{\partial \epsilon}{\partial k_p} \frac{\partial}{\partial k_q} \left(\tau \frac{\partial \epsilon}{\partial k_j} \right) \varepsilon_{lpq} d^3k \qquad \ldots.2.79$$

$e > 0$ for electron and ε_{lpq} is the permutation tensor defined in equation 2.29.

$$\sigma_{ij} = 0 \quad \text{unless } i=j \qquad \ldots.2.81$$

$$\sigma_{ijl} = 0 \quad \text{unless } i \neq j \neq l \neq i \qquad \ldots.2.82$$

The Hall coefficient is related to the conductivity coefficients 2.81 and 2.82 by

$$\rho_{ijl} = \frac{\sigma_{ijl}}{\sigma_{ii}\,\sigma_{jj}} \qquad \ldots.2.83$$

The expansion is useful when the magnetic field is not large enough to prevent convergence.

2.9 Evaluation of the tensor components of conductivity for quadratic energy surfaces.

When the relaxation time is dependant only on energy $(\tau = b\epsilon^{\lambda})$ the evaluation of the integrals 2.78 and 2.79 gives

$$\sigma_{ii} = -\frac{ab}{m_i^2} \int \epsilon^{\lambda} \frac{\partial f_o}{\partial \epsilon}\, d\epsilon \int \frac{k_i^2\, dS}{|\text{grad}\,\epsilon|} \qquad \ldots.2.84$$

where $\epsilon = \frac{\hbar^2}{2}\left[\frac{k_1^2}{m_1} + \frac{k_2^2}{m_2} + \frac{k_3^2}{m_3}\right]$

and dS is an element of constant energy surface.

When $m_1 = m_2$ and m_3 is the long axis of the ellipsoid

$$\sigma_{11} = \sigma_{22} = A m_3^{1/2} F_{\lambda+1/2}(\eta^*) \qquad \ldots.2.85$$

$$\sigma_{33} = \frac{A m_1}{m_3^{1/2}} F_{\lambda+1/2}(\eta^*) \qquad \ldots.2.86$$

with $\eta^* = \zeta / kT$ $\ldots.2.87$

$$F_p(\eta^*) = \int_0^\infty \frac{x^p \, dx}{1 + \exp(x - \eta^*)} \qquad \ldots.2.88$$

is the Fermi integral

$$A = ab 2^{7/2} \pi (\lambda + 3/2)(kT)^{(\lambda+3/2)} 3^{-1} \qquad \ldots.2.89$$

and $$a = \frac{e^2}{4\pi^3 \hbar^3} \qquad \ldots.2.90$$

$$\sigma_{123} = -B \frac{m_3^{1/2}}{m_1} F_{2\lambda+1/2}(\eta^*) \qquad \ldots.2.91$$

$$\sigma_{231} = -B \frac{1}{m_3^{1/2}} F_{2\lambda+1/2}(\eta^*) \qquad \ldots.2.92$$

$$\left.\begin{aligned} \sigma_{123} &= -\sigma_{213} \\ \sigma_{231} &= \sigma_{312} = -\sigma_{132} = -\sigma_{321} \end{aligned}\right\} \qquad \ldots.2.93$$

$$B = ab^2 d 2^{1/2} 3^{-1} \pi (2\lambda + 3/2)(kT)^{(2\lambda+3/2)} \qquad \ldots.2.94$$

$$d = \frac{e}{c} \qquad \ldots.2.95$$

Using equations 2.83 it is found that all the Hall coefficients are equal for a single ellipsoidal valley.

$$\rho_{ijl} = R = -\frac{B}{A^2} \frac{1}{m_1 m_3^{1/2}} \frac{F_{2\lambda+1/2}}{F^2_{\lambda+1/2}} \qquad \ldots.2.96$$

The carrier density is given by the products of the density of states term.

$$n(\epsilon)\Delta\epsilon = \frac{2}{(2\pi)^3} \int d^3k \qquad \ldots.2.97$$

with the carrier distribution function $f_o(\epsilon)$

$$n = \int_o^\infty n(\epsilon) f_o(\epsilon)\, d\epsilon = \int_{\epsilon=0}^{\epsilon=\infty} f_o(\epsilon)\, d^3k \qquad \ldots.2.98$$

$$= \frac{1}{2\pi^2} \left(\frac{2kT}{\hbar^2}\right)^{3/2} m_1 m_3^{1/2} F_{1/2}(\eta^*) \qquad \ldots.2.99$$

Substituting n into equation 2.96 gives

$$R = -\frac{1}{nec} \cdot \frac{3}{2} \frac{(2\lambda+3/2)}{(\lambda+3/2)^2} \cdot \frac{F_{1/2}(\eta^*) F_{2\lambda+1/2}(\eta^*)}{\left[F_{\lambda+1/2}(\eta^*)\right]^2} \qquad \ldots.2.100$$

with $e > 0$ for electrons.

If partial mobilities associated with the directions of the principal axes of the ellipsoid are defined by

$$\mu_i = \frac{e\langle\tau\rangle}{m_i} \qquad \ldots 2.101$$

$$= \frac{2}{3} eb(\lambda+3/2) \frac{(kT)^\lambda}{m_i} \frac{F_{\lambda+1/2}(\eta^*)}{F_{1/2}(\eta^*} \qquad \ldots 2.102$$

then $\sigma_{ii} = ne\mu_i$ $\ldots 2.103$

2.10 The relation between Q, R, and σ

The weak field Nernst coefficient is obtained from equation 2.63 for the single carrier isotropic case.

$$Q = \frac{1}{TeH} \frac{K_1H_2 - K_2H_1}{K_1^2} \qquad \ldots 2.104$$

$$= bk \frac{(kT)^\lambda}{m} f(F_p) \qquad \ldots 2.105$$

where $\ldots 2.106$

$$f(F_p) = \frac{(3/2+\lambda)(5/2+2\lambda)F_{\lambda+1/2}(\eta^*)F_{2\lambda+3/2}(\eta^*) - (3/2+2\lambda)(5/2+\lambda)F_{\lambda+3/2}(\eta^*)F_{2\lambda+1/2}(\eta^*)}{(3/2+\lambda)^2\left[F_{\lambda+1/2}(\eta^*)\right]^2}$$

Equation 2.105 together with

$$\sigma = ne\mu \qquad \ldots 2.107$$

and $$R = -\frac{1}{nec}\frac{3}{2}\frac{(3/2+2\lambda)}{(3/2+\lambda)^2}\frac{F_{2\lambda+1/2}(\eta^*)F_{1/2}(\eta^*)}{[F_{\lambda+1/2}(\eta^*)]^2} \qquad \ldots 2.108$$

give $$Q = -\lambda\frac{k}{e}aR\sigma \qquad \ldots 2.109$$

where $$a = \frac{1}{\lambda}\left[\frac{5/2+2\lambda}{3/2+2\lambda}\frac{F_{2\lambda+3/2}}{F_{2\lambda+1/2}} - \frac{5/2+\lambda}{3/2+\lambda}\frac{F_{\lambda+3/2}}{F_{\lambda+1/2}}\right] \qquad \ldots 2.110$$

a = 1 when non-degenerate statistics are applicable and is zero for full degeneracy. $a\lambda = 0$ when $\lambda = 0$

The expression for a for values of $\lambda = -1/2, 1/2, 3/2$ are given in table 1 and are plotted for values $-12 < \frac{\zeta}{kT} < 12$ in graph 1.

λ	$-1/2$	$1/2$	$3/2$
a	$4\frac{F_1}{F_0} - 6\frac{F_{1/2}}{F_{-1/2}}$	$\frac{14}{5}\frac{F_{5/2}}{F_{3/2}} - 3\frac{F_2}{F_1}$	$\frac{22}{27}\frac{F_{9/2}}{F_{7/2}} - \frac{8}{9}\frac{F_3}{F_2}$

TABLE 1.

2.11 The Thermoelectric Power.

The thermoelectric power for a single carrier is derived from equation 2.64.

$$\alpha = \frac{k}{e}\left\{\frac{A_{13}}{kT} + V^*\right\} \qquad \ldots.2.64$$

For the weak field case

$$\alpha = -\frac{1}{kT}\left[\frac{K_1 H_2 + H_1 K_2}{K_1^2}\right] + \frac{\zeta}{kT} \qquad \ldots.2.111$$

where H_i and K_i are given in equations 2.48, 2.49, 2.59 and 2.60. The substitution gives

$$\alpha_n = -\frac{k}{e}\left\{\frac{5/2+\lambda}{3/2+\lambda} \cdot \frac{F_{\lambda+3/2}(\eta^*)}{F_{\lambda+1/2}(\eta^*)} - \eta^*\right\} \qquad \ldots.2.112$$

for electrons. $(e>0)$

For holes $\alpha_p = -\alpha_n(\zeta^*)$ substituting ~~for~~ ζ^* for η^*

The partial thermoelectric powers are not directional (34) if the relaxation time is of the form $\tau = b\epsilon^{\lambda}$ as has been assumed.

2.12 The Nernst Coefficient.

The weak field Nernst coefficient for two carrier conduction with a single ellipsoidal energy surface for each band can be written as the sum

of two terms

$$Q_{yx} = Q^{a}_{yx} + Q^{c}_{yx} \qquad \ldots.2.113$$

where Q^{a}_{yx} is the bipoler contribution caused by carrier flow along the temperature gradient and subsequent recombination. Q^{c}_{yx} is the contribution due to individual carriers.

$$Q^{a}_{yx} = \lambda k \left[\frac{-a_n R_n n^2 \mu_x \mu_y + a_p R_p p^2 \nu_x \nu_y}{n\mu_x + p\nu_x} \right] \qquad \ldots.2.114$$

where n refers to electrons and p to holes

$$R_n = -\frac{1}{nec} \frac{3}{2} \frac{2\lambda + 3/2}{(\lambda + 3/2)^2} \frac{F_{1/2}(\eta^*) F_{2\lambda+1/2}(\eta^*)}{\left[F_{\lambda+1/2}(\eta^*)\right]^2} \qquad \ldots.2.115$$

and $$R_p = -R_n(S^*) \qquad \ldots..2.116$$

with S^* replacing η^* and p replacing n in 2.115

η^* and S^* are the reduced Fermi levels for holes and electrons respectively. μ_i and ν_i are electron and hole partial mobilities.

$$Q^{c}_{yx} = \frac{e(nR_n\mu_x - pR_p\nu_x) np \mu_y \nu_y (\alpha_n - \alpha_p)}{(n\mu_x + p\nu_x)(n\mu_y + p\nu_y)} \qquad \ldots..2.117$$

Both Q^a_{yx} and Q^c_{yx} are independent of carrier densities for the intrinsic case $n = p$.

For the particular case of a single ellipsoidal Fermi surface for each band the Nernst coefficient can be plotted if the Fermi levels of each carrier and the energy overlap of the bands are known. The ellipsoids for a particular crystal are situated in general in accordance with crystal symmetry and the coefficients 2.78 and 2.79 are then summed over all the valleys. The details are presented in a later chapter.

The isotropic Nernst coefficient however can be plotted for the various scattering parameters when some assumptions are made. When $n = p$ and the mobility ratio is unity the isotropic Nernst coefficient is

$$Q = Q^a + Q^c \qquad \ldots 2.118$$

$$Q^a = \frac{\lambda k n}{2}\left[-a_n R_n + a_p R_p\right]\mu \qquad \ldots 2.119$$

$$Q^c = \frac{ne}{4}\left[R_n - R_p\right]\left[\alpha_n - \alpha_p\right]\mu \qquad \ldots 2.120$$

and the useful quantity (35)

$$Q_1 = \frac{Q}{\mu}\frac{e}{k} = \frac{\lambda e n}{2}\left(-a_n R_n + a_p R_p\right) + \frac{ne^2}{4k}\left(R_n - R_p\right)\left(\alpha_n - \alpha_p\right) \qquad \ldots 2.121$$

can be plotted. This is done in graph 2 for values of $\lambda = -1/2, 0, 1/2, 3/2$ and for the Fermi level lying mid way between the valance and conduction band edges.

The quantity Q can be plotted for various crystals only when the band overlap and Fermi level of either the electrons or the holes are known.

CHAPTER 3

Graphite.

If an anisotropic material is used in a semiconducting energy converter the tensor components of conductivity must be summed over all the energy extreme in the Brillouin zone of the reciprocal lattice.

As the distribution of Fermi surfaces is determined by the symmetry of a particular crystal it is not possible to proceed to a general formulation of the transport coefficients. A particular model must be chosen.

As an illustration of the technique, graphite has the advantages that its Fermi surface is well defined, that there is available sufficient information on its transport properties to make a final estimate of its figure of merit and that the results for some orientations reduce to the isotropic case described in chapter 2.

3.1 The Crystal Lattice of Graphite.

The lattice points of the graphite crystal are shown in Figure 3.1. The carbon atoms are arranged in two distinct layers which are alternately repeated and are obtained from each

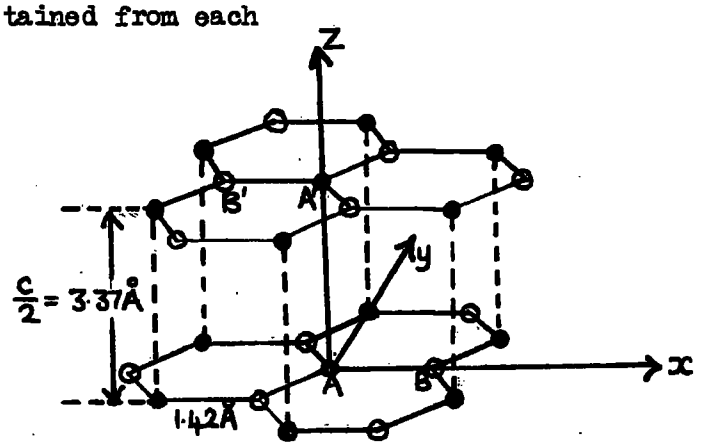

Fig. 3.1 The Graphite Crystal Lattice.

other by a translation along a triad (Z) axis and a rotation about this axis through 180°. In each plane the atoms are arranged in regular hexagons of side 1.42A (36). There are two types of atom, categorised with respect to their environment,; one with atoms above and below in adjacent planes, the other being above and below hexagon centres. They are denoted A and B type atoms respectively. The interlayer spacing is 3.37 A (36).

3.2 The Reciprocal Lattice of Graphite.

A set of basic vectors $\underline{a}_i$ (i = 1,2,3) of the graphite lattice is

$$\underline{a}_1=\left(\frac{a\sqrt{3}}{2}, -\frac{a}{2}, 0\right),\ \underline{a}_2=(0, a, 0) \quad \text{and} \quad \underline{a}_3=(0, 0, c)$$

where the origin of coordinates and the quantities a and c are shown in Figure 3.1. The unit cell encloses four atoms. The reciprocal lattice is defined by the vectors $\underline{b}_j$ (j = 1,2,3) satisfying the relation,

$$\underline{a}_i \cdot \underline{b}_j = 2\pi \delta_{ij}.$$

δ_{ij} is the Kronecker delta

The solution is

$$\underline{b}_1=\frac{2\pi(\underline{a}_2 \wedge \underline{a}_3)}{\underline{a}_1\cdot(\underline{a}_2 \wedge \underline{a}_3)},\quad \underline{b}_2=\frac{2\pi(\underline{a}_3 \wedge \underline{a}_1)}{\underline{a}_1\cdot(\underline{a}_2 \wedge \underline{a}_3)},\quad \underline{b}_3=\frac{2\pi(\underline{a}_1 \wedge \underline{a}_2)}{\underline{a}_1\cdot(\underline{a}_2 \wedge \underline{a}_3)}$$

$$\text{or } \underline{b}_1=\left[\frac{4\pi}{a\sqrt{3}}, 0, 0\right],\quad \underline{b}_2=\left[\frac{2\pi}{a\sqrt{3}}, \frac{2\pi}{a}, 0\right],\quad \underline{b}_3=\left[0, 0, \frac{2\pi}{c}\right]$$

The three $\underline{b}_j$ vectors define a right hexagonal cylinder shown in cross section in Figure 3.2

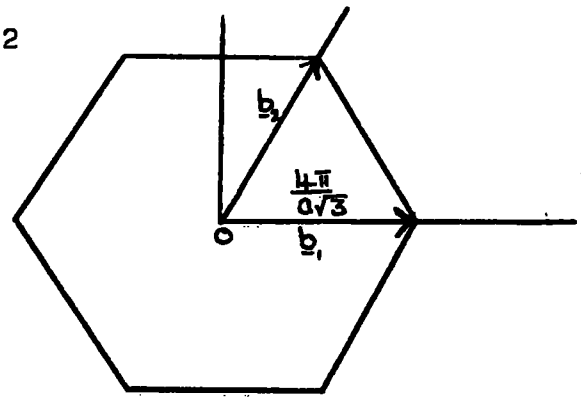

Fig. 3.2 Cross section of the graphite reciprocal lattice.

3.3 The Band Structure of Graphite.

The large anisotropy of the graphite crystal suggested that the band structure would not greatly differ from that of a two dimensional layer. Thus the early papers (37, 38, 39) first established the two dimensional structure and extended the method to include the interaction between layers. Although these calculations erroneously predicted a zero band gap implying no free carriers at zero absolute temperature they did serve to locate the Fermi level. This lay in the region of the edges of the hexagonal prism which is the Brillouin zone. As the actual overlap is small this is also where most of the current carriers are located and further studies (40, 41) have been confined to the neighbourhood of the zone edges.

3.4 The Band Structure of a Single Graphite Layer.

In isolation the carbon atom has the electronic configuration $1s^2 2s^2 2p^2$ with the $1s$ electrons forming the ion core and the remaining four electrons

being loosely bound valence electrons. When arranged in a graphite layer one of the $2s$ electrons is excited to the $2p_z$ state in a process of "hybridisation" (42). The $2s, 2p_x$ and $2p_y$ valence electrons form covalent bonds with valence electrons of three neighbouring atoms leaving the $2p_z$ electron loosely bound.

In a tight binding approximation involving only nearest neighbours Wallace (37) pointed out that a linear combination of hybrid orbitals corresponding to the $2s, 2p_x$ and $2p_y$ states gives rise to even (σ) eigen-states and that a linear combination of atomic orbitals gives an odd (π) eigenstate. The labelling even and odd is with respect to reflection in the layer plane. There are four bands for each of the two atoms in the two dimensional unit cell. Of these, six are σ-bands. Three of these are normally occupied and three unoccupied. They are separated by a gap of about $5ev$ in which there are two π-bands and the Fermi level. The lower π-band is designated the valence band and the upper π-band is the conduction band.

Wallace (37) considered only the π-bands and neglected all but nearest neighbour interactions. His solution for the energy in the vicinity of the Brillouin zone corners is

$$E(\underline{k}_u + \underline{K}) = E_u \pm \frac{\sqrt{3}}{2}\gamma_0 a K + O(K^2) \qquad \ldots. 3.1$$

where $\underline{K} = \underline{k} - \underline{k}_u$ is the wave vector $\underline{k}$ measured from U, the Brillouin zone corner of wave vector $\underline{Ku}$ and Eu is the energy at U. $O(k^2)$ indicates

powers of K greater than unity.

$$\gamma_0 = -\int d\tau \psi^*_{2p_z}(\underline{r}-\underline{r}_A)(V-V_{at})\psi_{2p_z}(\underline{r}-\underline{r}_B) > 0$$

is the resonance integral for nearest neighbours with the $2p_z$ atomic orbitals.

V is the periodic one electron potential

V_{at} is the potential of an isolated atom.

$\underline{r}_A$ and $\underline{r}_B$ are the position vectors of the atoms A and B in figure 1.

$a = 2.46\text{Å}$ is the primitive lattice vector.

A two-fold degeneracy occurs at U, when K = 0. This is verified in later more extensive papers (40,43,44) and is attributed to crystal symmetry.

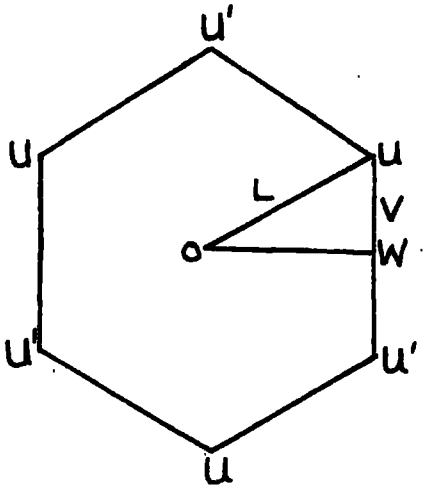

Fig 3.3 The Brillouin Zone of a single graphite layer.

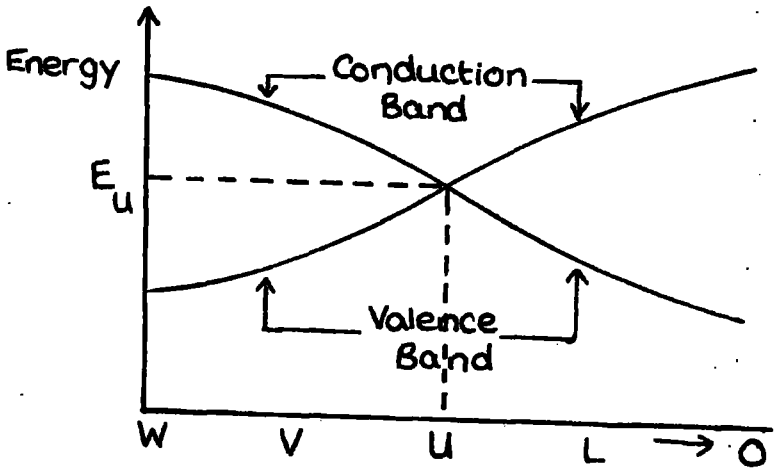

Fig. 3.4 Variation of energy in the bands along the path OLUVW

The energy is plotted in Figure 3.4 for the path OLUVW in the two dimensional Brillouin zone shown in Figure 3.3. The constant energy contours in the

neighbourhood of U are circles and for given γ_0 the π- bands form touching cones.

3.5 The Three Dimensional Band Structure of Graphite.

The three dimensional Brillouin Zone is shown in Figure 3.5

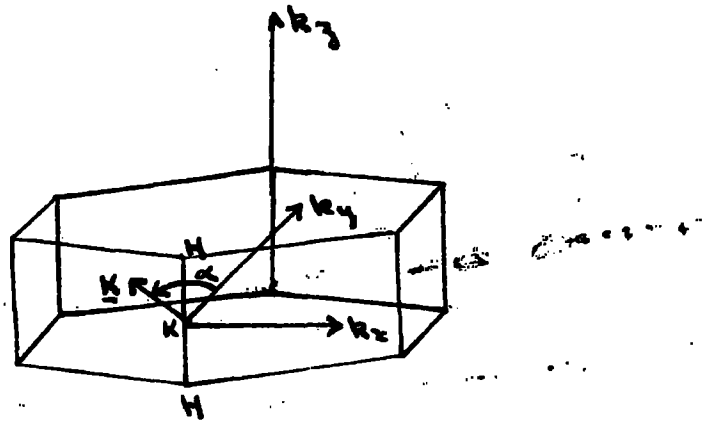

Fig 3.5 The Brillouin zone of Graphite.

Wallace (37) used a similar approach to obtain the three dimensional band structure. Retaining only resonance integrals between the atoms A and B, and A and A' of figure 3.1 the energy in the vicinity of HKH is (41)

$$E(\sigma,\xi)=E_3\pm\tfrac{1}{2}\gamma_1\Gamma\pm\left[\left(\tfrac{1}{2}\gamma_1\Gamma\right)^2+\left(\gamma_0\sigma\right)^2\right]^{1/2} \qquad \ldots\ldots 3.2$$

where $\sigma=\frac{\sqrt{3}}{2}aK$, $\Gamma=2\cos\left(\frac{\xi}{2}\right)$ and $\xi=k_z c_0$

$$\gamma_1 = -\int d\tau \psi^*_{2p_z}(\underline{r}-\underline{r}_A)(V-V_{at})\psi_{2p_z}(\underline{r}-\underline{r}_{A'}) > 0$$

is the resonance integral between A and A' atoms.

The energy for the four bands described by equation 3.2 is plotted in figure 3.6 along the zone edge and figure 3.7 shows the hyperbolic variation of energy with σ away from the zone edge for a particular value of ξ .

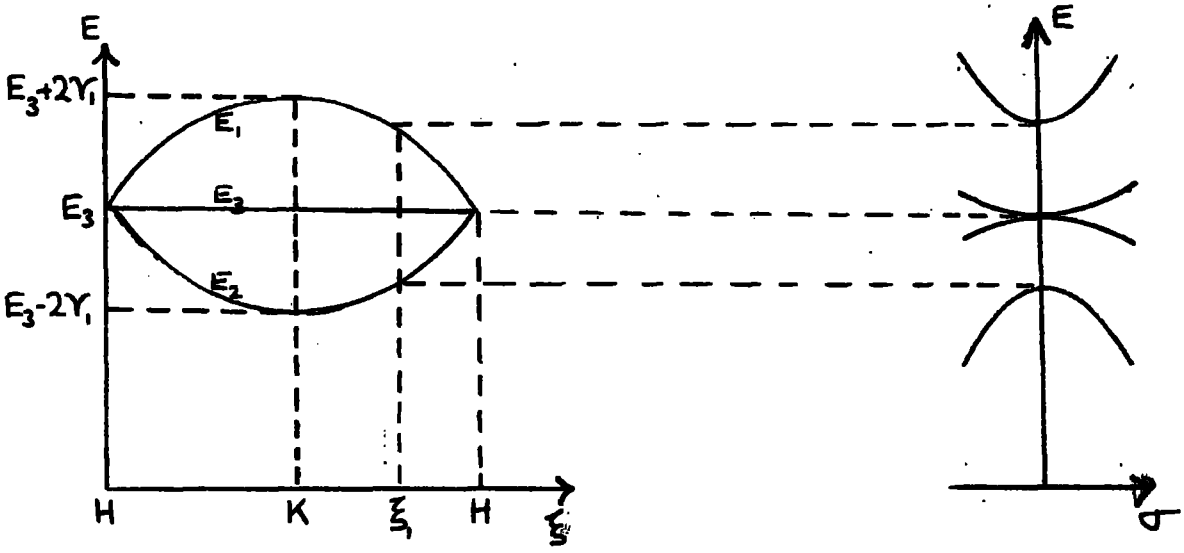

Figure 3.6 The four bands of equation 3.2 plotted for $\sigma = 0$

Figure 3.7 The variation of the bands away from the zone edge.

Two of the bands are degenerate all along the zone edge and four fold degeneracy occurs at the zone corners H. Later calculations show that a more exact treatment taking more than nearest neighbours into account causes a variation of E_3 along the zone edge and produces vertical overlap of the bands E_3 . The resulting qualitative discrepancy has caused the approach

to be abandoned in favour of a group theoretical treatment which takes advantage of the fact that only the vicinity of the zone edges needs to be studied.

A combination of group theoretical analysis of the wave functions and perturbation theory was used by Slonczewski and Weiss (40) to determine the three dimensional band structure. They observed from previous results that only the π - bands needed to be discussed in the neighbourhood of the edges of the hexagonal Brillouin zone and approximated to the three dimensional wave functions by taking linear combinations of $2p_z$ atomic orbitals corresponding to the two layers in the unit cell.

The four functions

$$\psi_1 = \frac{1}{\sqrt{2}}\left\{\sum_n \exp(in\xi)u_2(\underline{r}-n\underline{c}_o)+\sum_n \exp[i(n+\tfrac{1}{2})\xi]\hat{u}_1(\underline{r}-n\underline{c}_o)\right\}$$

$$\psi_2 = \frac{1}{\sqrt{2}}\left\{\sum_n \exp(in\xi)u_2(\underline{r}-n\underline{c}_o)-\sum \exp[i(n+\tfrac{1}{2})\xi]\hat{u}_1(\underline{r}-n\underline{c}_o)\right\}$$

$$\psi_{31} = \sum_n \exp[i(n+\tfrac{1}{2})\xi]\hat{u}_2(\underline{r}-n\underline{c}_o)$$

$$\psi_{32} = \sum_n \exp(in\xi)u_1(\underline{r}-n\underline{c}_o)$$

are shown by Slonczewski and Weiss (40) to form the basis of an irreducible representation of the wave vector group corresponding to any point on the zone edge.

u_1 and u_2 are the two basic functions corresponding to a corner of the two

dimensional zone. They represent the two two-dimensional states and are degenerate at the zone corners. $\hat{u}_1$ and $\hat{u}_2$ are similarly defined for the other layer in the three dimensional unit cell.

The Hamiltonian H is reduced to that corresponding to the four wave functions ψ_1, ψ_2, ψ_{31} and ψ_{32} and is given in a convenient notation by McClure (41). This involves the sim constants associated with the band structure of graphite.

$$H = \left[\begin{array}{cccc|c} E_1 & 0 & H_{13} & H_{13}^* & :\psi_1 \\ 0 & E_2 & H_{23} & -H_{23}^* & :\psi_2 \\ H_{13}^* & H_{23}^* & E_3 & H_{33} & :\psi_{31} \\ H_{13} & -H_{23} & H_{33}^* & E_3 & :\psi_{32} \end{array}\right]$$

with $E_1 = \gamma_1 \Gamma + \Delta$

$$E_2 = -\gamma_1 \Gamma + \Delta$$

$$E_3 = \gamma_2 (1 + \cos \xi) = \tfrac{1}{2} \gamma_2 \Gamma^2$$

$$H_{13} = \frac{1}{\sqrt{2}} (-\gamma_0 + \gamma_4 \Gamma) \sigma \exp(i\alpha)$$

$$H_{23} = \frac{1}{\sqrt{2}} (\gamma_0 + \gamma_4 \Gamma) \sigma \exp(i\alpha)$$

$$H_{33} = \gamma_3 \Gamma \sigma \exp(i\alpha)$$

$$\alpha = \tan^{-1}\left(\frac{K_x}{K_y}\right), \sigma = \frac{\sqrt{3}}{2} a_0 |\underline{K}|$$

$$\xi = k_z c_0, \Gamma = 2 \cos\left(\frac{\xi}{2}\right)$$

$\underline{K}$ is the displacement from the edge HKH in a plane perpendicular to the zone corner.

Only the lowest terms are retained in this calculation both for the rapidly converging series expansions and in the terms involving σ. Higher order terms in σ are shown by Mc.Clure (41) to have only a small quantitative effect.

The four bands are derived from the secular equation.

$$|H - EI| = 0$$

This quartic equation is not solved explicitly in the first instance but can be factored when γ_3 and γ_4 are set equal to zero.

Then the bands are

$$E = \tfrac{1}{2}(E_1 + E_3) \pm \left[\tfrac{1}{4}(E_1 - E_3)^2 + \gamma_0^2 \sigma^2\right]^{1/2}$$

$$E = \tfrac{1}{2}(E_2 + E_3) \pm \left[\tfrac{1}{4}(E_2 - E_3)^2 + \gamma_0^2 \sigma^2\right]^{1/2}$$

For a given value of k_z they form a set of hyperboloids of revolution two of which touch at $\sigma = 0$. A description of the bands is shown in Figure 3.7 based on estimates of the relative magnitudes of γ_1, γ_2 and Δ. Figure 3.8a shows the variation along a zone edge for $\sigma = 0$ and figure 3.8b. the variation with σ for a given value of ξ. The latter have rotational symmetry about the energy axis. Mc.Clure has drawn a three dimensional plot of energy against the vectors k_z and $\underline{K}$ for these bands in the four parameter model.

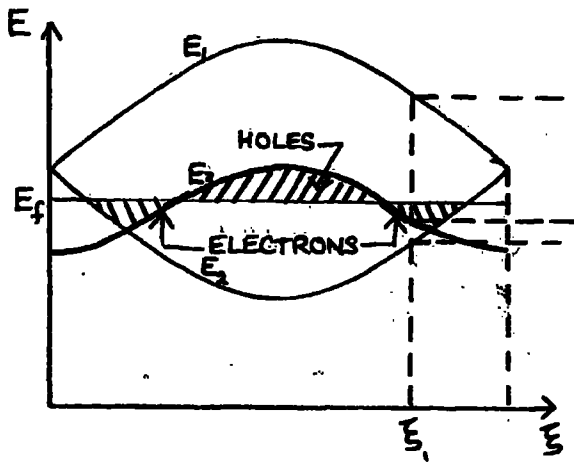

Figure 3.8a The four energy bands ($\gamma_3=\gamma_4=0$) Variation shows along a zone edge.

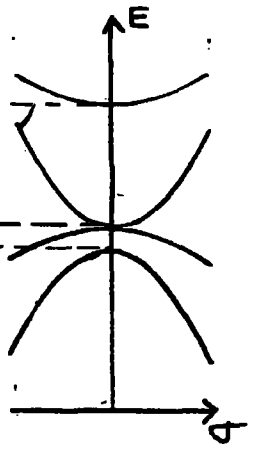

Figure 3.8b The variation with σ away from the edge for a particular

The inclusion of γ_4 does not affect the qualitative description since it merely modifies γ_0 but γ_3 causes a warping of the energy surfaces and further degeneracies for energies in the vicinity of E_3. Examination of the two bands derived from ψ_{31} and ψ_{32} under the assumption that E_3 was well removed from E_1 and E_2 led Mc.Clure (41) to predict additional overlapping of the bands in the planes $\alpha = \frac{1}{3}\pi$. This trigonal warping together with his three dimensional four parameter plot gave the Fermi surface drawn in Figure 3.9

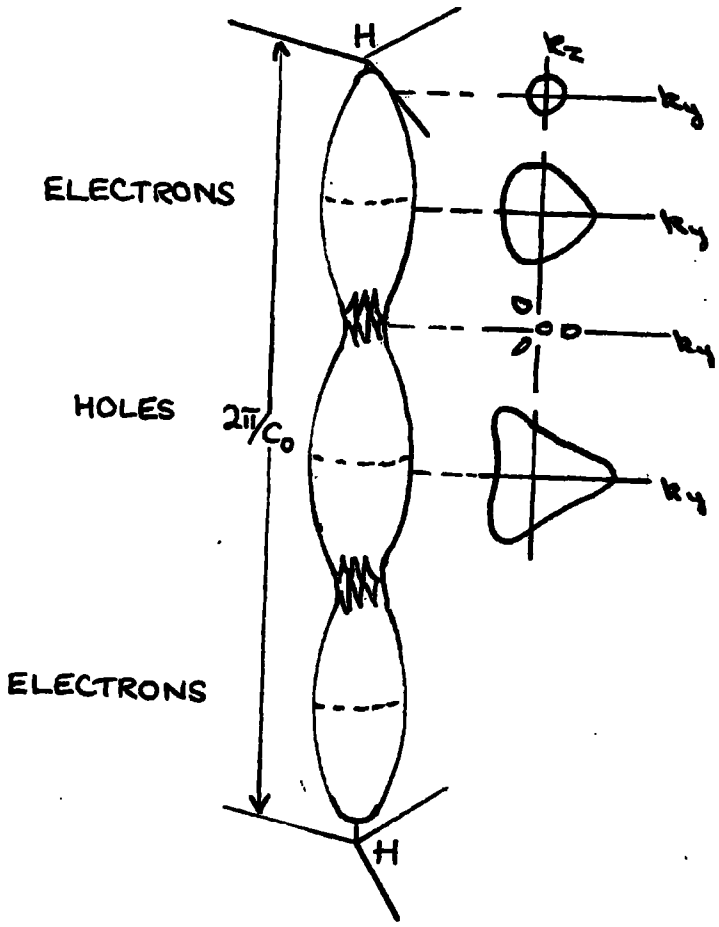

Figure 3.9 Description of the Fermi surface in graphite showing, in exagerated form, the cross sectional areas. The length to width ratio of the "ellipsoids" is about 13:1

A review of the literature on the band structure of graphite has been published by Haering and Mrowzowski (45) and the features predicted in the Fermi surfaces have been verified experimentally by Soule (46) and Dresselhaus and Mavroides (47).

CHAPTER 4.

The Nernst Coefficient in Graphite.

The complex band structure of graphite and the position and shape of the Fermi surfaces make the formal analysis of its transport properties very unwieldy. A rather more simple calculation is made in which the Fermi surfaces are taken to be ellipsoidal. This is justified in view of the large length to width ratio of the Fermi surfaces and amounts to neglecting the small amount of warping caused by interactions between the atoms B and B' of figure 3.1. The anisotropic transport coefficients so obtained are expressed in their simplest form in terms of partial mobilities and are used to evaluate the Nernst coefficient in the weak field approximation. Exact statistics are used.

4.1 The Conductivity Coefficients in Graphite.

From the description of the band structure given in chapter 3 it is seen that graphite has eighteen energy extrema placed in three layers of six with each extrema on an edge of the hexagonal Brillouin zone. The central plane contains the six extrema associated with the valence band while the remaining twelve extrema are in the conduction band. The Fermi surfaces are assumed to be ellipsoids centred on these extrema and each major axis is along a zone edge. The configuration is shown in figure 4.1

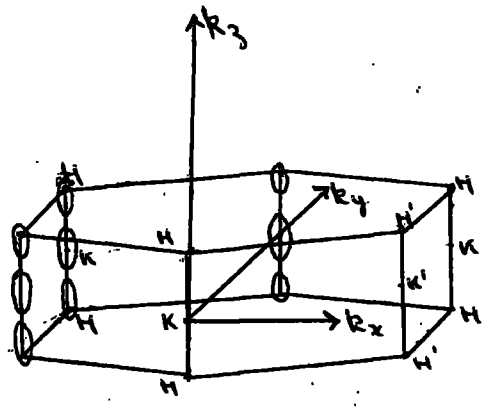

Figure 4.1 The Fermi surfaces in Graphite.

An orthogonal set of axes may be chosen for an arbitrary ellipsoid, denoted the i^{th} valley (i = 1.....12 for electrons and i = 1.....6 for holes) which coincides with the crystal axes. The energy in the vicinity of the extrema is then

$$E = E_o + \frac{\hbar^2}{2}\left\{\frac{k_1^2}{m_1} + \frac{k_2^2}{m_2} + \frac{k_3^2}{m_3}\right\} \qquad \ldots\ 4.1$$

with $m_1 = m_2$. k is the displacement in wave vector space from the zone edge. E_o is the extremum value of energy.

As the results for the valence band differ only by a numerical factor from those for the conduction band the general discussion is now confined to electrons.

The remaining ellipsoids for the conduction band are generated from the ellipsoid by the following set of real orthogonal matrices R^y .

$$\begin{bmatrix} 1 & 0 & 0 \\ 0 & 1 & 0 \\ 0 & 0 & 1 \end{bmatrix} \quad \begin{bmatrix} C & -S & 0 \\ S & C & 0 \\ 0 & 0 & 1 \end{bmatrix} \quad \begin{bmatrix} -C & -S & 0 \\ S & -C & 0 \\ 0 & 0 & 1 \end{bmatrix} \quad \begin{bmatrix} -1 & 0 & 0 \\ 0 & -1 & 0 \\ 0 & 0 & +1 \end{bmatrix}$$

$$\begin{bmatrix} -C & S & 0 \\ -S & -C & 0 \\ 0 & 0 & 1 \end{bmatrix} \quad \begin{bmatrix} C & S & 0 \\ -S & C & 0 \\ 0 & 0 & 1 \end{bmatrix} \quad \begin{bmatrix} -1 & 0 & 0 \\ 0 & -1 & 0 \\ 0 & 0 & -1 \end{bmatrix} \quad \begin{bmatrix} -C & S & 0 \\ -S & -C & 0 \\ 0 & 0 & -1 \end{bmatrix}$$

$$\begin{bmatrix} C & S & 0 \\ -S & C & 0 \\ 0 & 0 & -1 \end{bmatrix} \quad \begin{bmatrix} 1 & 0 & 0 \\ 0 & 1 & 0 \\ 0 & 0 & -1 \end{bmatrix} \quad \begin{bmatrix} C & -S & 0 \\ S & C & 0 \\ 0 & 0 & -1 \end{bmatrix} \quad \begin{bmatrix} -C & -S & 0 \\ S & -C & 0 \\ 0 & 0 & -1 \end{bmatrix}$$

where $C = \cos(\pi/3)$ and $S = \sin(\pi/3)$

The phenomenological coefficients are obtained by summing the tensor components corresponding to each valley in the manner described by Drabble and Wolfe (48).

The total conductivity coefficients are

$$\sigma_{pq} = \left\{ \sum_j R^{ij}_{pk} R^{ij}_{ql} \right\} a^i_{kk} a^i_{lu} \sigma^{(i)}_{ku} \qquad \ldots\ 4.2$$

$$\sigma_{pqr} = \left\{ \sum_j R^{ij}_{pk} R^{ij}_{ql} R^{ij}_{rm} \right\} a^i_{kk} a^i_{lu} a^i_{mv} \sigma^{(i)}_{kuv} \qquad \ldots\ 4.3$$

where the a^i_{ij}'s are the direction cosines of the principal axis system of the i^{th} ellipsoid relative to the crystal axes. In this case $[a^i_{ij}]$ is merely the unit matrix but any angle of tilt can be accommodated quite easily.

The tensor components for a single valley are given by equations 2.85 to 2.90 and 2.91 to 2.95 if the assumption that a power dependence of relaxation time on energy is made.

On carrying out the various summations the independent non-zero components of conductivity are

$$\sigma_{11} = 12 A m_3^{1/2} \qquad \ldots 4.4$$

$$\sigma_{33} = 12A \frac{m_1}{m_3^{1/2}} \qquad \ldots 4.5$$

$$\sigma_{11} = \sigma_{22} \qquad \ldots 4.6$$

$$\sigma_{123} = -12B \frac{m_3^{1/2}}{m_1} \qquad \ldots 4.7$$

$$\sigma_{231} = -12B \cdot \frac{1}{m_3^{1/2}} \qquad \ldots 4.8$$

$$\sigma_{ijk} = -\sigma_{jik} \qquad \ldots 4.9$$

$$\sigma_{231} = \sigma_{312} \qquad \ldots 4.10$$

The partial Hall coefficients are

$$\rho_{ijk} = \frac{\sigma_{ijk}}{\sigma_{ii}\sigma_{jj}} = -\frac{B}{12A^2} \cdot \frac{1}{m_1 m_3^{1/2}} \qquad \ldots 4.11$$

Which have a single value for the particular symmetry of graphite.

The factor 12 is replaced by 6 for the valence band and the parameters associated with holes are used in the appropriate places.

4.2 The Nernst Coefficient.

The substitution of the conductivity coefficients into equation 2.73 gives the weak field Nernst coefficient for the six orientations obtained by permutation of the orthogonal axes x, y and z. The Nernst coefficients for these orientations are displayed in table 4.1. Table 4.2 shows the Nernst coefficients in their simplest form in terms of partial mobilities and Fermi levels.

The relations

$$\mu_i = \frac{2}{3} eb_n (kT)^{\lambda} \frac{F_{\lambda+\frac{1}{2}}(\eta^*)}{F_{\frac{1}{2}}(\eta^*)} \cdot \frac{1}{m_{in}} \qquad \text{for electrons} \quad \ldots 4.12$$

$$\text{and } \nu_i = \frac{2}{3} eb_p (kT)^{\lambda} \frac{F_{\lambda+\frac{1}{2}}(\zeta^*)}{F_{\frac{1}{2}}(\zeta^*)} \frac{1}{m_{ip}} \qquad \text{for holes} \quad \ldots 4.13$$

are used.

Table 4.1 Weak field approximations for the Nernst coefficient in Graphite

y	x	Q_{yx}
1	2	$\frac{\lambda k}{e}\cdot\frac{2a_n B_n \frac{m_{3n}^{1/2}}{m_{1n}} + a_p B_p \frac{m_{3p}^{1/2}}{m_{1p}}}{2A_n m_{3n}^{1/2} + A_p m_{3p}^{1/2}} + \frac{2A_n A_p m_{3n}^{1/2} m_{3p}^{1/2}\left\{\frac{B_n}{A_n m_{1n}} + \frac{B_p}{A_p m_{1p}}\right\}\bar{\alpha}}{\left\{2A_n m_{3n}^{1/2} + A_p m_{3p}^{1/2}\right\}^2}$
2	1	
1	3	$\frac{\lambda k}{e}\cdot\frac{\frac{2a_n B_n}{m_{3n}^{1/2}} + \frac{a_p B_p}{m_{3p}^{1/2}}}{2A_n\frac{m_{1n}}{m_{3n}^{1/2}} + A_p\frac{m_{1p}}{m_{3p}^{1/2}}} + \frac{2A_n A_p m_{3n}^{1/2} m_{3p}^{1/2}\left\{\frac{B_n}{A_n m_{3n}} + \frac{B_p}{A_p m_{3p}}\right\}\bar{\alpha}}{\left\{2A_n\frac{m_{1n}}{m_{3n}^{1/2}} + A_p\frac{m_{1p}}{m_{3p}^{1/2}}\right\}\left\{2A_n m_{3n}^{1/2} + A_p m_{3p}^{1/2}\right\}}$
2	3	
3	1	$\frac{\lambda k}{e}\cdot\frac{\frac{2a_n B_n}{m_{3n}^{1/2}} + \frac{a_p B_p}{m_{3p}^{1/2}}}{2A_n m_{3n}^{1/2} + A_p m_{3p}^{1/2}} + \frac{2A_n A_p \frac{m_{1n}m_{1p}}{m_{3n}^{1/2}m_{3p}^{1/2}}\left\{\frac{B_n}{A_n m_{1n}} + \frac{B_p}{A_p m_{1p}}\right\}\bar{\alpha}}{\left\{2A_n\frac{m_{1n}}{m_{3n}^{1/2}} + A_p\frac{m_{1p}}{m_{3p}^{1/2}}\right\}\left\{2A_n m_{3n}^{1/2} + A_p m_{3p}^{1/2}\right\}}$
3	2	

The relaxation time $\tau = b\epsilon^{\lambda}$ where ϵ is the energy

$$A_n = ab_n 2^{1/2}\pi(\lambda+3/2)(kT)^{(\lambda+3/2)}3^{-1}$$

$$B_n = ab_n^2 d\, 2^{1/2} 3^{-1}\pi(2\lambda+3/2)(kT)^{(2\lambda+3/2)}$$

$$a = e^2/4\pi^3\hbar^3 \quad , \quad d = \frac{e}{c}$$

a_n is defined by equation 2.110

$\bar{\alpha} = \alpha_p - \alpha_a$ the difference of partial thermoelectric powers.

Table 4.2 The weak field Nernst coefficient in graphite in terms of the partial mobilities.

y	x	Q_{yx}
1 2	2 1	$\frac{3}{2c}(2\lambda+3/2)\left[\frac{\lambda k}{e}\left\{\frac{2n a_n \mu_1^2 \rho_-^\lambda + p a_p \nu_1^2 \rho_+^\lambda}{2n\mu_1 + p\nu_1}\right\} + \left\{\frac{2np\mu_1\nu_1(\mu_1\rho_-^\lambda + \nu_1\rho_+^\lambda)\bar{\alpha}}{(2n\mu_1 + p\nu_1)^2}\right\}\right]$
1 2	3 3	$\frac{3}{2c}(2\lambda+3/2)\left[\frac{\lambda k}{e}\left\{\frac{2n a_n \mu_1 \mu_3 \rho_-^\lambda + p a_p \nu_1 \nu_3 \rho_+^\lambda}{2n\mu_3 + p\nu_3}\right\} + \left\{\frac{2np\mu_1\nu_1(\mu_3\rho_-^\lambda + \nu_3\rho_+^\lambda)\bar{\alpha}}{(2n\mu_1+p\nu_1)(2n\mu_3+p\nu_3)}\right\}\right]$
3 3	1 2	$\frac{3}{2c}(2\lambda+3/2)\left[\frac{\lambda k}{e}\left\{\frac{2n a_n \mu_1 \mu_3 \rho_-^\lambda + p a_p \nu_1 \nu_3 \rho_+^\lambda}{2n\mu_1 + p\nu_1}\right\} + \left\{\frac{2np\mu_3\nu_3(\mu\rho_-^\lambda + \nu_1\rho_+^\lambda)\bar{\alpha}}{(2n\mu_1+p\nu_1)(2n\mu_3+p\nu_3)}\right\}\right]$

$$\rho_-^\lambda = \frac{F_{1/2}(\eta^*)F_{2\lambda+1/2}(\eta^*)}{[F_{\lambda+1/2}(\eta^*)]^2} \qquad \rho_+^\lambda = \frac{F_{1/2}(\zeta^*)F_{2\lambda+1/2}(\zeta^*)}{[F_{\lambda+1/2}(\zeta^*)]^2}$$

The electron and hole densities are $N = 12n$ and $P = 6p$

In tables 4.1 and 4.2 x is the direction of the electric field
y is the direction of thermal gradient
and $\underline{H}$ is in the z - direction.

Since $m_1 = m_2$ for both electrons and holes it follows from equations 4.12 and 4.13 that $\mu_1 = \mu_2$ and $\nu_1 = \nu_2$ and this has been used in deriving the coefficients in table 4.2.

In pure graphite the scattering parameter, λ, has the value $\lambda = -\frac{1}{2}$ while in pyrolytic graphite it has been suggested (35) that boundary scattering, for which $\lambda = 0$, gives a better explanation of the experimental behaviour of the Nernst coefficient. In both materials the electron and hole densities are very nearly equal and $2n \doteq \rho$.

4.3 The Nernst Coefficient for acoustic mode scattering

The coefficients of table 4.2 may be written as the sum of two terms, one, Q_-, negative and the other, Q_+, positive. The components are given in table 4.3.

y	x	Q_-	Q_+
1	2	$-\frac{3}{8c}\frac{k}{e}\mu_1\left[\frac{a_n\rho_-^{-1/2}+a_p E^2\rho_+^{-1/2}}{1+E}\right]$	$\frac{3}{4c}\mu_1\cdot\frac{E(\rho_-^{1/2}+E\rho_+^{-1/2})}{(1+E)^2}\bar{\alpha}$
2	1		
1	3	$-\frac{3}{8c}\frac{k}{e}\mu_1\left[\frac{a_n\rho_-^{-1/2}+a_p EF\rho_+^{-1/2}}{1+F}\right]$	$\frac{3}{4c}\mu_1\cdot\frac{E(\rho_-^{-1/2}+F\rho_+^{-1/2})}{(1+E)(1+F)}\bar{\alpha}$
2	3		
3	1	$-\frac{3}{8c}\frac{k}{e}\mu_3\left[\frac{a_n\rho_-^{-1/2}+a_p EF\rho_+^{-1/2}}{1+E}\right]$	$\frac{3}{4c}\mu_3\cdot\frac{F(\rho_-^{-1/2}+E\rho_+^{-1/2})}{(1+E)(1+F)}\bar{\alpha}$
3	2		

$$\rho_-^{-1/2} = \frac{F_{1/2}(\eta^*)F_{-1/2}(\eta^*)}{[F_0(\eta^*)]^2} \quad ; \quad \rho_-^{-1/2}(\zeta^*) = \rho_+^{-1/2}$$

$E = \frac{\nu_1}{\mu_1}$ and $F = \frac{\nu_3}{\mu_3}$. It is assumed that the electron and hole densities are equal (49) so that $2n = p$

When the degenerate limit is approached

$$a_n \rightarrow a_p \rightarrow 0$$

and

$$p_-^{-1/2} \rightarrow p_+^{-1/2} \rightarrow 4/3$$

For non-degeneracy

$$a_n \rightarrow a_p \rightarrow 1$$

and

$$p_-^{-1/2} \rightarrow p_+^{-1/2} \rightarrow \pi/2$$

The general value of a is given by equation 2.110.

For degenerate material Q_- is zero in each case since the degeneracy factor $a \rightarrow 0$

In the degenerate limit

$$Q_{\substack{12\\21}} \rightarrow Q_{\substack{13\\23}} \rightarrow \frac{\mu_1}{c} \frac{E}{1+E} \bar{\alpha} \qquad \ldots 4.14$$

and

$$Q_{\substack{31\\32}} \rightarrow \frac{\mu_3}{c} \frac{F}{1+F} \bar{\alpha} \qquad \ldots 4.15$$

The non-degenerate limits are

$$Q_{\substack{12\\21}} = \frac{\mu_1}{c} \frac{3\pi}{8} \left[-\frac{1}{2} \frac{k}{e} \frac{1+E^2}{1+E} + \frac{E}{1+E} \bar{\alpha} \right] \qquad \ldots 4.16$$

$$Q_{\substack{13\\23}} = \frac{\mu_1}{c} \frac{3\pi}{8} \left[-\frac{1}{2} \frac{k}{e} \frac{1+EF}{1+F} + \frac{E}{1+E} \bar{\alpha} \right] \qquad \ldots 4.17$$

$$Q_{\substack{31\\32}} = \frac{\mu_3}{c} \frac{3\pi}{8} \left[-\frac{1}{2} \frac{k}{e} \frac{1+EF}{1+E} + \frac{F}{1+F} \bar{\alpha} \right] \qquad \ldots 4.18$$

The mobility ratio E is very close to unity (49) over the temperature range 0 - 300°K and making the assumption that this, together with c-direction mobility ratio F, are unity, gives the following non-degenerate limits for the Nernst coefficient.

$$Q_{\substack{12\\21}} = Q_{\substack{13\\23}} = \frac{\mu_1}{c}\ \frac{3\pi}{16}\ \frac{k}{e}\left[3 + \frac{\epsilon_g}{kT}\right] \qquad \ldots 4.19$$

$$Q_{\substack{31\\32}} = \frac{\mu_3}{c}\ \frac{3\pi}{16}\ \frac{k}{e}\left[3 + \frac{\epsilon_g}{kT}\right] \qquad \ldots 4.20$$

where $-\epsilon_g$ is the energy overlap of the conduction and valence bands.

Q_{12} is plotted against the temperature, T, in graph 4.
The values of a - axis mobility are taken from graph 3 which is a smooth curve through the three points given by McClure (49).

Q_{12}^{+} rises as mobility rises with decreasing temperature until the partial thermoelectric powers begin to fall.

Q_{12}^{-} increases with mobility from 22% of Q_{12}^{+} at 298°K to 60% at 10°K thereafter diminishing to zero due to the degeneracy factor a.

The overall effect is to produce a maximum in the $Q_{12}\left(=Q_{21}=Q_{12}^{-}=Q_{12}^{+}\right)$ curve at about 80° .

If the assumption is made that the c-direction mobility ratio F has a value of about unity over the temperature range 0 - 300° K then $Q_{13}=(Q_{23})$ has a similar behaviour to Q_{12}. However, Q_{31} is proportional to μ_3 which is three to four orders of magnitude less than μ_1 (50) and the Nernst coefficient in this orientation is too small to be worth further analysis in the context of providing a large figure of merit.

The quantity $\frac{Q_{12}}{\mu_1}\frac{e}{k}$ is plotted in graph 5 for values of the reduced energy gap from -10 to +10.

4.4 The Nernst Coefficient for Boundary Scattering ($\lambda=0$)

The term denoted by in the discussion of the coefficients for acoustic mode scattering is, in this case, zero and the Nernst coefficients simplify considerably to

$$Q_{\substack{12\\21}} = Q_{\substack{13\\23}} = \frac{1}{c}\mu_1\frac{E}{1+E}\bar{\alpha} \qquad \ldots 4.21$$

$$Q_{\substack{31\\32}} = \frac{1}{c}\mu_3\frac{F}{1+F}\bar{\alpha} \qquad \ldots 4.22$$

and to

$$Q_{\substack{12\\21}} = Q_{\substack{13\\23}} = \frac{1}{c}\frac{\mu_1}{2}\bar{\alpha} \qquad \ldots 4.23$$

$$Q_{\substack{31\\32}} = \frac{1}{c}\frac{\mu_3}{2}\bar{\alpha} \qquad \ldots 4.24$$

when the mobility ratios are unity.

The non-degenerate limits are

$$Q_{\substack{12\\21}} = Q_{\substack{13\\23}} = \frac{1}{c}\frac{\mu_1}{2}\left[5+\frac{\epsilon_g}{kT}\right] \qquad \ldots 4.25$$

$$Q_{\substack{31\\32}} = \frac{1}{c}\frac{\mu_3}{2}\left[5+\frac{\epsilon_g}{kT}\right] \qquad \ldots 4.26$$

Q_{12} is plotted for $\lambda=0$ in graph 6 against temperature over the range $0<T<400^{\circ}K$ The behaviour is similar to Q_{12} for $\lambda=-\frac{1}{2}$ but

as there is no negative contribution the maximum of the curve has a value about three times larger for boundary scattering.

$\frac{\Omega_{12}}{\mu_1}\frac{e}{k}$ is plotted in graph 5 for the range $-10 < x < 10$ where x is the reduced energy gap.

CHAPTER-5.

The Conductivity Tensor in Strong Magnetic Fields.

The field dependent expressions for the figure of merit have terms $\mu^2H^2/(1+\mu^2H^2)$ which has a saturation value of unity for high values of μH. In addition, the electronic component K_e of thermal conductivity in inversely proportional to the magnetic field and becomes increasingly small compared with the lattice component, K_L, for large μH particularly at low temperatures ($<10^oK$). It is useful, therefore, to examine the high field behaviour of the conductivity tensor.

5.1 The Electrical Conductivity.

The components of electrical conductivity are extracted from

$$\underline{I} = \frac{e}{4\pi^3\hbar^3}\int \text{grad}\,\epsilon \frac{\partial f_o}{\partial \epsilon}\,\phi\, dV \qquad \ldots. 5.1$$

which may be written in tensor form

$$i_i = \sigma_{ik}(\underline{H})E_k \qquad \ldots. 5.2$$

where the σ_{ik} are the tensors of conductivity expressed as integrals in equation (5.1). The symbols have the meanings ascribed to them in chapter 1.

For a general power dependence of relaxation time on energy

$$\tau = b\epsilon^{\lambda} \qquad \ldots. 5.3$$

the integrals reduce to the form

$$J \equiv \int \frac{\epsilon^n d\epsilon}{\epsilon^{2\lambda} + kT\omega^2} \qquad \ldots. 5.4$$

with $$\omega = vK^{1/2}\left(H_1^2 + H_2^2 + KH_3^2\right)^{1/2} \qquad \ldots\ 5.5$$

$$K = m_3/m_1 \qquad \ldots\ 5.6$$

and $$v = \frac{eb}{c(kT)^{1/2} m_3} \qquad \ldots\ 5.7$$

$\underline{H} \equiv (H_1, H_2, H_3)$ is the magnetic field.

Except for boundary scattering ($\lambda = 0$), when the denominator of J is independent of energy it is necessary to use digital computation for exact statistics. An analytical solution can be obtained for lattice scattering ($\lambda = -1/2$) when the limits of degeneracy or non-degeneracy set in.

In expanded notation, Φ (equation 2.37) is given by (51)

$$\Phi = \frac{-\frac{e\tau}{m_1}\left\{P_1 + \frac{e\tau}{c}\left[\frac{P_2 H_3}{m_2} - \frac{P_3 H_2}{m_3}\right] + \left(\frac{e\tau}{c}\right)^2 \left(\frac{H_1}{m_2 m_3}\right)\left(P_1 H_1 + P_2 H_2 + P_3 H_3\right)\right\} E_1}{1 + \left(\frac{e\tau}{c}\right)^2 \left[\frac{H_1^2}{m_2 m_3} + \frac{H_2^2}{m_3 m_1} + \frac{H_3^2}{m_1 m_2}\right]} + \qquad \ldots\ 5.8$$

and two other terms obtained by cyclic permutation of indices.

$\underline{E} = (E_1, E_2, E_3)$ is the electric field.

$\underline{P} = (P_1, P_2, P_3)$ is the momentum vector.

The components of conductivity are obtained by comparison of equations (5.2) and (5.3). For example

$$\sigma_{11} = \frac{-e^2}{4\pi^3 \hbar^3} \int \frac{\frac{P_1}{m_1^2}\frac{\partial f_0}{\partial \epsilon}\tau\left\{P_1 + \frac{e\tau}{c}\left(\frac{P_2 H_3}{m_2} - \frac{P_3 H_2}{m_3}\right) + \left(\frac{e\tau}{c}\right)^2 \left(P_1 H_1 + P_2 H_2 + P_3 H_3\right)\right\} dV}{\left\{1 + \left(\frac{\tau}{b}\right)^2 kT\omega^2\right\}} \qquad \ldots\ 5.9$$

The element $dV = \frac{d\epsilon dS}{|grad\epsilon|}$, the integration being performed first over a constant energy surface and then with respect to energy. Integration over the surface S yields integrals of the form

$$J_i \equiv \int \frac{P_i P_j \, dS}{\left\{\frac{P_1^2}{m_1^2} + \frac{P_2^2}{m_2^2} + \frac{P_3^2}{m_3^2}\right\}^{1/2}} \qquad \ldots 5.10$$

which are zero unless i = j. With $m_1 = m_2$

$$J_1 = J_2 = 2^{1/2} 3^{-1} \pi m_1^2 m_3^{1/2} \epsilon^{3/2} \qquad \ldots 5.11$$

and $$J_3 = 2^{1/2} 3^{-1} \pi m_1 m_3^{3/2} \epsilon^{3/2} \qquad \ldots 5.12$$

Then $$\sigma_{11} = -a 2^{1/2} 3^{-1} \pi m_3^{1/2} \int \frac{\partial f_0}{\partial \epsilon} \frac{\epsilon^{3/2} \tau \left\{1 + \left(\frac{e\tau}{c}\right)^2 \frac{H_1^2}{m_2 m_3}\right\} d\epsilon}{1 + \left(\frac{\tau}{b}\right)^2 kT\omega^2} \qquad \ldots 5.13$$

where $a = \frac{e^2}{4\pi^3 \hbar^3}$.

The other components are similar and are given explicity only as results in the relevant sections.

5.2 Boundary Scattering.

The field dependent terms in equation (5.13) can be taken outside the integral as the relaxation time in this case is independent of energy.

$$\tau = b_0 \qquad \ldots 5.14$$

Then $$\sigma_{11} = -a 2^{1/2} 3^{-1} \pi m_3^{1/2} b_0 \frac{\left\{1 + \left(\frac{eb_0}{c}\right)^2 \frac{H_1^2}{m_2 m_3}\right\}}{1 + kT\omega^2} \int \frac{\partial f_0}{\partial \epsilon} \epsilon^{3/2} d\epsilon \qquad \ldots 5.15$$

$$= ne^2 \frac{b_e}{m_1} \left\{ \frac{1+\left(\frac{eb_e}{c}\right)^2 \frac{H_1^2}{m_2 m_3}}{1+kT\omega^2} \right\} \quad \ldots\ldots 5.16$$

$$= ne\mu_1(\underline{H}) \quad \ldots\ldots 5.17$$

where $$\mu_1(\underline{H}) = \mu_1(0) \frac{1+\mu_1(0)\mu_3(0)\frac{H_1^2}{c^2}}{1+\frac{\mu_1(0)\mu_3(0)}{c^2}\left(H_1^2+H_2^2+\frac{\mu_1(0)}{\mu_3(0)}H_3^2\right)} \quad \ldots\ldots 5.18$$

$\ldots\ldots 5.19$

$\mu_i(0) = \frac{eb_e}{m_i}$ is the zero field mobility for boundary scattering.

and $m_1 = m_2$

5.3 Acoustic Mode Scattering.

In this case the relaxation time, and hence the field dependent factors, in the integral of equation (5.13) are energy dependent. The resulting integrals are complex and further analytical ~~process~~ progress is made only when the limits of non-degeneracy or degeneracy are applicable. σ_{11} is derived below for the non-degenerate case and the results for the other components of electrical conductivity for this case and for complete degeneracy will be quoted.

From equation (5.13)

$$\sigma_{11} = -ab_1 2^{1/2} 3^{-1} \pi m_3^{1/2} \int \frac{df_e}{d\epsilon} \frac{\left\{\epsilon^2 + \epsilon\left(\frac{eb_1}{c}\right)^2 \frac{H_1^2}{m_2 m_3}\right\}}{\epsilon + kT\omega^2} d\epsilon \quad \ldots\ldots 5.20$$

where $\tau = b_1 \epsilon^{-1/2}$ 5.21

The integrals required for the evaluation of the tensor components when non-degenerate statistics are used $\left(f_o \rightarrow \exp\left[-\left(\frac{\epsilon - \epsilon_f}{kT}\right)\right]\right)$ are (51,52)

$$\int \frac{\partial f_o}{\partial \epsilon} \frac{\epsilon^2}{\epsilon + kT\omega^2} d\epsilon = -P\alpha(\omega) \quad .... 5.22$$

$$\int \frac{\partial f_o}{\partial \epsilon} \frac{\epsilon^{3/2}}{\epsilon + kT\omega^2} d\epsilon = -P(kT)^{-1/2}\beta(\omega) \quad .... 5.23$$

$$\int \frac{\partial f_o}{\partial \epsilon} \frac{\epsilon}{\epsilon + kT\omega^2} d\epsilon = -P(kT)^{-1}\gamma(\omega) \quad .... 5.24$$

where $P = 2^{1/2}\pi^{3/2}\hbar^3 n m_1^{-1} m_3^{-1/2} (kT)^{-1/2}$

$$\alpha(\omega) = 1 - \omega^2 + \omega^4 \exp(\omega^2) E(\omega^2) \quad .... 5.25$$

$$\beta(\omega) = \pi^{1/2}\left[\tfrac{1}{2} - \omega^2 + \pi^{1/2}\omega^3 \exp(\omega^2) F(\omega)\right] \quad .... 5.26$$

$$\gamma(\omega) = 1 - \omega^2 \exp(\omega^2) E(\omega^2) \quad .... 5.27$$

$$E(x) = \int_x^\infty \frac{e^{-t}}{t} dt \quad .... 5.28$$

$$F(x) = 1 - \frac{2}{\pi^{1/2}} \int_0^x \exp(-t^2)\, dt \quad .... 5.29$$

Then

$$\sigma_{11} = uK\left[\alpha(\omega) + v^2 H_1^2 K \gamma(\omega)\right] \quad .... 5.30$$

$$= n e \mu_1(\underline{H}) \qquad \ldots 5.31$$

where

$$\mu_1(H) = \mu_1(0)\left[\alpha(\omega) + \frac{9\pi}{16}\mu_1(0)\mu_3(0)\frac{H_1^2}{c^2}\gamma(\omega)\right] \qquad \ldots 5.32$$

$$\mu_i(0) = \frac{4eb_i}{3m_i(\pi kT)^{1/2}}$$

is the zero field mobility for lattice scattering and $m_1 = m_2$

$$\mu = \frac{4e^2 b_1 n}{3m_3(\pi kT)^{1/2}} \qquad \ldots 5.33$$

The complete set of tensor components for both acoustic mode scattering and boundary scattering are given in table 5.1

	Boundary Scattering ($\lambda=0$)	Acoustic Mode Scattering ($\lambda=-1/2$)
σ_{11}	$ne^2\frac{b_0}{m_1}\left\{1+\left(\frac{eb_0}{c}\right)^2\frac{H_1^2}{m_1m_3}\right\}\left\{1+kT\omega^2\right\}^{-1}$	$uK[\alpha(\omega)+v^2H_1^2K\gamma(\omega)]$
σ_{22}	$ne^2\frac{b_0}{m_1}\left\{1+\left(\frac{eb_0}{c}\right)^2\frac{H_2^2}{m_1m_3}\right\}\left\{1+kT\omega^2\right\}^{-1}$	$uK[\alpha(\omega)+v^2H_2^2K\gamma(\omega)]$
σ_{33}	$ne^2\frac{b_0}{m_3}\left\{1+\left(\frac{eb_0}{c}\right)^2\frac{H_3^2}{m_1^2}\right\}\left\{1+kT\omega^2\right\}^{-1}$	$u[\alpha(\omega)+v^2H_3^2K^2\gamma(\omega)]$
σ_{12}	$\frac{ne^3}{c}\frac{b_0^2}{m_1^2}\left\{-H_3+\frac{eb_0}{cm_3}H_1H_2\right\}\left\{1+kT\omega^2\right\}^{-1}$	$vuK^2[-\beta(\omega)H_3+vH_1H_2\gamma(\omega)]$
σ_{23}	$\frac{ne^3}{c}\frac{b_0^2}{m_1m_3}\left\{-H_1+\frac{eb_0}{cm_1}H_2H_3\right\}\left\{1+kT\omega^2\right\}^{-1}$	$vuK[-\beta(\omega)H_1+vH_2H_3K\gamma(\omega)]$
σ_{31}	$\frac{ne^3}{c}\frac{b_0^2}{m_1m_3}\left\{-H_2+\frac{eb_0}{cm_1}H_1H_3\right\}\left\{1+kT\omega^2\right\}^{-1}$	$vuK[-\beta(\omega)H_2+vH_3H_1K\gamma(\omega)]$
	Arbitrary degree of degeneracy and field strength	Non-degenerate statistics - arbitrary field strength.

Table 5.1 Tensor Components of Electrical Conductivity $\sigma_{ik}(\underline{H})=\sigma_{ki}(-\underline{H})$

Summation over all the valleys of the conduction band is reduced to multiplication by 12 for both sets of tensor components as for the weak field case. However, it must be noted that the magnetic field is fixed in direction and must be replaced after each transformation by the original field referred to the new co-ordinates. For the valence band the factor is 6. The terms involving $\beta(\omega)$ cancel in the summation.

The components of interest for the evaluation of the figure of merit are the diagonal elements with the magnetic field in particular directions, which simplify considerably the components shown in table 5.1. The necessary components reduce to those given in tables 5.2 and 5.3.

y	x	H	σ_x conduction band.	σ_x valence band.	ω
1	2	(0,0,H)	$12uK\alpha(\omega)$	$6uK\alpha(\omega)$	vKH
2	1	(0,0,H)	$12uK\alpha(\omega)$	$6uK\alpha(\omega)$	vKH
1	3	(0,H,0)	$12u\alpha(\omega)$	$6u\alpha(\omega)$	$vK^{1/2}H$
2	3	(H,0,0)	$12u\alpha(\omega)$	$6u\alpha(\omega)$	$vK^{1/2}H$
3	1	(0,H,0)	$12uK\alpha(\omega)$	$6uK\alpha(\omega)$	$vK^{1/2}H$
3	2	(H,0,0)	$12uK\alpha(\omega)$	$6uK\alpha(\omega)$	$vK^{1/2}H$

Table 5.2 Conductivity components for acoustic mode scattering.

1	2	(0,0,H)	$12ne^2\frac{b_o}{m_1}(1+kT\omega^2)^{-1}$	$6pe^2\frac{b_o}{m_1}(1+kT\omega^2)^{-1}$	vKH
2	1	(0,0,H)	$12ne^2\frac{b_o}{m_1}(1+kT\omega^2)^{-1}$	$6pe^2\frac{b_o}{m_1}(1+kT\omega^2)^{-1}$	vKH
1	3	(0,H,0)	$12ne^2\frac{b_o}{m_3}(1+kT\omega^2)^{-1}$	$6pe^2\frac{b_o}{m_3}(1+kT\omega^2)^{-1}$	$vK^{1/2}H$
2	3	(H,0,0)	$12ne^2\frac{b_o}{m_3}(1+kT\omega^2)^{-1}$	$6pe^2\frac{b_o}{m_3}(1+kT\omega^2)^{-1}$	$vK^{1/2}H$
3	1	(0,H,0)	$12ne^2\frac{b_o}{m_1}(1+kT\omega^2)^{-1}$	$6pe^2\frac{b_o}{m_1}(1+kT\omega^2)^{-1}$	$vK^{1/2}H$
3	2	(H,0,0)	$12ne^2\frac{b_o}{m_1}(1+kT\omega^2)^{-1}$	$6pe^2\frac{b_o}{m_1}(1+kT\omega^2)^{-1}$	$vK^{1/2}H$

Table 5.3 Conductivity components for boundary scattering.

The appropriate effective masses and constants b_0 and b_1 are used in tables 5.2 and 5.3 for the conduction band and the valence band and, throughout, $m_1 = m_2$.

The saturation values of the principal components of conductivity are given in terms of zero field mobilities in table 5.4. It is assumed that the total conductivity is the sum of the individual components due to the valence band and the conduction band and that electron and hole densities are equal.

The saturation value of $\alpha(\omega)$ for high fields is

$$\lim_{H\to\infty} \alpha(\omega) = \frac{1}{\omega^2} + O\left(\frac{1}{\omega^3}\right) \qquad \ldots 5.34$$

y	x	H	σ_{xx} boundary scattering	σ_{xx} acoustic mode scattering non-degenerate limit.
1	2	(0,0,H)	$\frac{ne}{H^2}\left(\frac{1}{\mu_1}+\frac{1}{\nu_1}\right)$	$\frac{32}{9\pi}\frac{ne}{H^2}\left(\frac{1}{\mu_1}+\frac{1}{\nu_1}\right)$
2	1	(0,0,H)		
1	3	(0,H,0)		
2	3	(H,0,0)		
3	1	(0,H,0)	$\frac{ne}{H^2}\left(\frac{1}{\mu_3}+\frac{1}{\nu_3}\right)$	$\frac{32}{9\pi}\frac{ne}{H^2}\left(\frac{1}{\mu_3}+\frac{1}{\nu_3}\right)$
3	2	(H,0,0)		

Table 5.4 The high field saturation values of σ_{xx} in terms of zero field mobilities.

$$\mu_i = \frac{eb_o}{m_i} \quad \text{for boundary scattering}$$

$$= \frac{4eb_1}{3m_i(\pi k l)^{\frac{1}{2}}} \quad \text{for acoustic mode scattering.}$$

The fully degenerate limit of σ_{xx} for acoustic mode scattering is evaluated by approximating f_o by the function.

$$\left.\begin{aligned} f_o &= 1 \quad \text{for } 0 \leq \epsilon \leq \epsilon_f \\ &= 0 \quad \text{for } \epsilon_f \leq \epsilon \end{aligned}\right\} \qquad \ldots\ldots 5.35$$

where ϵ_f is the Fermi level.

The expressions obtained are those of tables 5.4 with the factor replaced by unity.

5.4 The Thermal Conductivity.

The thermal conductivity K_T has two components K_L and K_ϵ due respectively to lattice vibrations and the current carriers. The latter, K_ϵ, has itself, contributions from holes K_h, electrons K_e and the bipolar effect K_{eh}. The electronic component is derived from the phenomenological equations in just the same manner as for the purely electrical coefficients. The detailed derivation for the anisotropic case is of no concern here, however, as it is observed from the isotropic expression for the simple two band model that its nature is such that it can be neglected in comparison with K_L when sufficiently large magnetic

fields are applied.

The expression for K_E is given by Klein (53,55)

$$K_E = T\left(\frac{k}{e}\right)^2 \left[\gamma_h \sigma_h + \gamma_e \sigma_e + \frac{\sigma_h \sigma_e}{\sigma_h + \sigma_e}\left(\delta_h + \delta_e - \frac{E_o}{kT}\right)^2\right] \quad \ldots\ldots 5.36$$

γ and δ are the following degeneracy factors.

$$\gamma = \frac{\lambda+7/2}{\lambda+1/2} \cdot \frac{F_{\lambda+5/2}}{F_{\lambda+1/2}} - \left[\frac{\lambda+5/2}{\lambda+3/2} \cdot \frac{F_{\lambda+3/2}}{F_{\lambda+1/2}}\right]^2 \quad \ldots\ldots 5.37$$

$$\delta = \frac{\lambda+5/2}{\lambda+3/2} \frac{F_{\lambda+3/2}}{F_{\lambda+1/2}} \quad \ldots\ldots 5.38$$

F_ρ is the Fermi integral.

Thus the electronic component of thermal conductivity is proportional overall to the electrical conductivity, which is expected from the simple Lorentz relation.

$$L = \frac{K_E}{\sigma T} \quad \ldots\ldots 5.39$$

Consequently, the high field behaviour of K_E is $\sim \frac{\sigma_o}{H^2}$ and each of the terms K_e, K_h, K_{eh} are negligible compared with K_L which depends only on the lattice vibrations and is field independent. These comments are pertinent for graphite at temperatures lower than about 10^oK when K_E becomes comparable with K_L and can be larger at

temperatures lower than about $2^{\circ}K$ (53). Above $10^{\circ}K$, K_L is much larger than K_E and the latter, even in the field free case, can be neglected.

The in-plane experimental behaviour of the thermal conductivity has been discussed by Mills (et alia) (35). At low temperatures K has a temperature dependence of T^2 and at high temperatures a T^{-1} dependence. A peak value of about 30 $W cm^{-1} {}^{\circ}K^{-1}$ occurs at about 140° and a value 20 $W cm^{-1} {}^{\circ}K^{-1}$ is recorded at $80^{\circ}K$ for their best sample. Experimental values of thermal conductivity are given in Table 5.5 for three of their samples.

Deposition Temperature ($^{\circ}C$)	Thermal Conductivity ($W cm^{-1} {}^{\circ}K^{-1}$)		
	at $80^{\circ}K$	Peak Value	Temp. of peak.
2700	6	13	195
2920	11	19	170
2980	20	31	144

Table 5.5 The a-direction thermal conductivity in pyrolytic graphite.

Experimental values of c-direction thermal conductivities are not available over a wide temperature range ($0 < T < 300^{\circ}K$) but values at $300^{\circ}K$ are quoted by Slack (54) and he provides an anisotropy ratio $K_{\perp}/K_{\parallel}$ over the range $0 < T < 300^{\circ}K$ for a particular sample, (P.G.-0) of pyrolytic graphite with a good degree of crystallite alignment. The subscripts $\perp$ and $\parallel$ refer to directions perpendicular and parallel to the c-direction.

His results indicate that $K_{\perp}/K_{\parallel}$ is temperature dependent, having an asymptotic low temperature value 2.25 and a value of 500 at $300^{\circ}K$. He concludes that at $300^{\circ}K$ this ratio would approach 1000 for a single crystal graphite.

5.5 The Figure of Merit.

The preceeding theory provides the information required for the evaluation of the figure of merit for graphite.

$$Z_E = (Q_{yx} H_z)^2 \frac{\sigma_{xx}}{K_{yy}} \qquad \ldots\ldots 5.40$$

Where x is the direction of the electric field and the thermal gradient is in the y-direction.

The general conclusions are:

1) The Nernst coefficient is independent of magnetic field.

11) The electrical conductivity is reduced by a factor $(1 + \mu^2 H^2)$ in the denominator on application of a magnetic field.

111) The electronic component of thermal conductivity is negligible compared with the lattice component K_L at temperatures greater than $20^{\circ}K$ and, for sufficiently high magnetic fields, in the range $0 < T \lesssim 20^{\circ}K$

from which

$$Z_E \sim \frac{\sigma_{ox}}{K_{L,y}} \left(\frac{\mu_x^2 H_z^2}{1 + \mu_x^2 H_z^2} \right) \qquad \ldots\ldots 5.41$$

The factor in brackets has the asymptotic value of unity for large values of μH and is 0.9 for magnetic fields of 0.35, 5, 35 Kilogauss at temperatures 4,80 and 300°K

The six components corresponding to table 5.4 are given in table 5.6 for boundary scattering with general statistics and in table 5.7 for acoustic mode scattering with non-degenerate statistics. The latter restriction on the degree of degeneracy could be removed if experimental values of field dependent electrical conductivity rather than zero field mobilities were available.

y	x	Z_E
1	2	$ne\mu_1 \frac{E}{1+E} \frac{\bar{\alpha}^2}{K_{L,1}}$
2	1	
1	3	
2	3	
3	1	$ne\mu_3 \frac{F}{1+F} \frac{\bar{\alpha}^2}{K_{L,3}}$
3	2	

Table 5.6 The figure of merit for boundary scattering. $(K_{L,1} = K_{L,2})$

y	x	Z_E
1	2	$ne\mu_1 \frac{2}{E(1+E)} \frac{1}{\pi} \left[-\frac{k}{2e}\rho_{a,E} + \frac{E}{1+E}\rho_E \bar{\alpha}\right]^2 \frac{1}{K_{L,1}}$
2	1	
1	3	$ne\mu_1 \frac{2(1+E)}{E(1+F)^2} \frac{1}{\pi} \left[-\frac{k}{2e}\rho_{a,EF} + \frac{E}{1+E}\rho_F \bar{\alpha}\right]^2 \frac{1}{K_{L,1}}$
2	3	
3	1	$ne\mu_3 \frac{2(1+F)}{F(1+E)^2} \frac{1}{\pi} \left[-\frac{k}{2e}\rho_{a,EF} + \frac{E}{1+F}\rho_E \bar{\alpha}\right]^2 \frac{1}{K_{L,3}}$
3	2	

Table 5.7 The figure of merit for acoustic mode scattering (assuming non-degenerate statistics for evaluation of the electrical conductivity)

$$\rho_{a,E} = a_n \rho_-^{-1/2} + a_p E^2 \rho_+^{-1/2}$$

$$\rho_{a,EF} = a_n \rho_-^{-1/2} + a_p EF \rho_+^{-1/2}$$

$$\rho_E = \rho_-^{-1/2} + E\rho_+^{-1/2}$$

$$\rho_F = \rho_-^{-1/2} + F\rho_+^{-1/2}$$

$\rho_-^{-1/2}$ and $\rho_+^{-1/2}$ are defined below table 4.3 and [illegible] "a" is defined by equation 2.110 and plotted for acoustic mode scattering in graph 1.

When the non-degenerate limits are inserted for $\rho_{a,E}$ and $\rho_{a,EF}$ the expressions of table 5.8 are obtained for acoustic mode scattering.

y	x	Z_E
1	2	$ne\mu_1 \frac{\pi}{4}\left(\frac{k}{e}\right)^2\left[3+\frac{\epsilon_g}{kT}\right]^2 \frac{1}{K_{L,1}}$
2	1	
1	3	
2	3	
3	1	$ne\mu_3 \frac{\pi}{4}\left(\frac{k}{e}\right)^2\left[3+\frac{\epsilon_g}{kT}\right]^2 \frac{1}{K_{L,3}}$
3	2	

Table 5.8 The non-degenerate limit for the figure of merit (acoustic mode scattering, mobility ratios E and F close to unity).

The evaluation of the figure of merit is most easily accomplished by reducing the expressions in tables 5.6 and 5.7 to a more compact form. The components for the orientation x = 2, y = 1 is

$$Z_{E(1,2)} = r\left(\frac{k}{e}\right)^2 Q_1^2 \frac{\sigma_o}{K_{L,1}} = Z_{E(2,1)} \qquad \ldots\ldots 5.42$$

where r is a degeneracy factor.

$r = 1$ for boundary scattering.

$= 32/9\pi$ for acoustic mode scattering with non-degenerate statistics.

A theoretical plot of $Q_{1,}$ is available in graph 5 for both boundary scattering and acoustic mode scattering. Mills et alia (35) provide experimental values of the ratio σ_o/K_L for temperatures down to 60° and extropolated values for lower temperatures.

$$\sigma_o = 2ne\mu_1 \qquad \ldots\ldots 5.43$$

is the zero field electrical conductivity for equal hole and electron densities. The values predicted for $Z_{E(1,2)}$ are given in table 5.9 for boundary scattering and acoustic mode scattering.

T(°K)	$(Q/\mu)_b$ $V°K^{-1}$	$(Q/\mu)_{am}$ $V°K^{-1}$	$\sigma_o/K_{L,1.}$	$(Z_E)_b$ $(°K^{-1})$	$(Z_E)_{am}$ $(°K^{-1})$
4	8.1×10^{-6}	4.9×10^{-6}	19.5×10^{5}	1.2×10^{-4}	0.47×10^{-4}
10	30×10^{-6}	9.8×10^{-6}	2.4×10^{5}	2.2×10^{-4}	0.23×10^{-4}
80	150×10^{-6}	87×10^{-6}	$.013 \times 10^{5}$	2.9×10^{-5}	0.98×10^{-5}

Table 5.9 _____ for both acoustic mode and boundary scattering.

The components $Z_{E(1,3)} = Z_{E(2,3)}$ are expected to be of the same magnitude as $Z_{E(1,2)}$ if the mobility ratio $F = \nu_3/\mu_3$ is about unity for the acoustic mode case. These components are identical for boundary scattering.

The ratio

$$\frac{Z_{E(1,2)}}{Z_{E(3,1)}} = \frac{\mu_1}{\mu_3} \cdot \frac{K_{L,3}}{K_{L,1.}} \qquad \ldots\ldots 5.44$$

is always greater than unity, since, according to Slack (54), the anisotropy in electrical conductivity is greater than that of the thermal conductivity.

The figures of merit in table 5.9 are not large enough to provide adequate cooling at any temperature the requirement being $\sim 10^{-20} K^{-1}$.

It is concluded that graphite does not provide a useful figure of merit in the usual orientation with the magnetic field perpendicular to the basal planes and that an increase is not obtained by directing the field parallel to the planes. The close agreement with experimental evidence suggests that the model used for the band structure is sufficient and that further refinement is unnecessary for this particular application of the thermo-galvanomagnetic effects.

Appendix 2A.

Derivation of the Boltzmann Equation.

Let $f(\underline{r}, \underline{k}, t)$ be the average number of carriers which are in a state described by position vector $\underline{r}$, wave vector $\underline{k}$ and time t. According to Liouville's theorem, $f(\underline{r}, \underline{k}, t)$ the distribution function of particles in an isolated system, is constant for motion along a path in phase space,

$$\frac{df}{dt} = \frac{\partial f}{\partial t} + \left(\frac{\partial f}{\partial t}\right)_{ext} + \left(\frac{\partial f}{\partial t}\right)_{coll} = 0 \qquad \ldots 2.A.1$$

$\left(\frac{\partial f}{\partial t}\right)_{ext}$ signifies changes in the distribution function due to the action of external forces, $\left(\frac{\partial f}{\partial t}\right)_{coll}$ represents changes due to scattering phenomena within the material and $\frac{\partial f}{\partial t}$ is the temporal change. In the steady state $\frac{\partial f}{\partial t} = 0$ and, since

$$\left(\frac{\partial f(r,k)}{\partial t}\right)_{ext} = -\left[\frac{dr}{dt}\,\nabla_r f + \frac{dk}{dt}\,\nabla_k f\right] \qquad \ldots 2.A.2$$

the equation for the distribution function becomes

$$\underline{v}\cdot\nabla_r f + \underline{F}\cdot\nabla_k f = \left(\frac{\partial f}{\partial t}\right)_{coll} \qquad \ldots 2.A.3$$

where $\underline{v} = \frac{dr}{dt}$ is the carrier velocity and $\underline{F} = \frac{\hbar\, dk}{dt}$ is the external force acting on the carrier. If the applied fields are electric, E, and magnetic, H,

$$\underline{F} = -e\left(\underline{E} + \tfrac{1}{c}\underline{v}\wedge\underline{H}\right) \qquad e > 0 \text{ for electrons} \qquad \ldots 2.A.4$$

Combination of equation 2. A. 3 and 2. A. 4 gives the Boltzmann equation.

$$-\frac{e}{\hbar}\left(\underline{E} + \frac{1}{c}\underline{v}\wedge\underline{H}\right) + \underline{v}\cdot\nabla_r f = \left(\frac{\partial f}{\partial t}\right)_{coll} \qquad \ldots 2.A.5$$

REFERENCES.

1) R.R. Heikes and R.W. Ure Thermoelectricity (Interscience: New York, London, 1961).

2) A.F. Ioffe Semiconductor Elements and Thermoelectric Cooling (London: Infosearch, 1957).

3) B.J. O'Brien and C.S. Wallace. J. App. Phys. 29,1010, 1958.

4) D.A. Wright Brit. J. App. Phys. 13, 583, 1962.

5) T.C. Harman and H.M. Honig. J. App. Phys. (a) 33, 3178, 1962 (b) 33, 3188, 1962; (c) 34, 189, 1963; (d) 34, 2215, 1963; (e) 34, 2225, 1963.
App. Phys. Letters. 1, 31, 1962.

6) C.F. Kooi, R.B. Horst, K.F. Cuff and S.R. Hawkins. J. App. Phys. 34, 1735, 1963.

7) R.T. Delves. Brit. J. App. Phys. 13, 440, 1962.

8) G. Smith and R. Wolfe. Bull. Am. Phys. Soc. 6, 13T, 1961.

9) M.R. El-Saden. J. App. Phys. 33, 1800, 1962.

10) B.V. Paranjape and J.S. Levinger. Phys. Rev. 120, 437, 1960.

11) H.B. Callen. Thermodynamics (J.Wiley and Sons, New York, 1960)

12) J.M. Honig and B.M. Tarmy. J. App. Phys. 35, 722, 1964.

13) C.A. Domenicali. J. App. Phys. . 25, 1310, 1954.

14) S.R. de Groot. Thermodynamics of Irresersible Phenomena (Interscience, New York, 1951)

15) L. Onsager. Phys. Rev. 37, 405, 1931.

16) A.C. Beer Galvanomagnetic Effects in Semiconductors. (Spp. 4 to Solid State Phys. 1963)

17) A.H. Wilson Theory of Metals (Cambridge U.P. 1953) Chapter 1.

18) I.M. Tsidil'kovskii. Thermomagnetic Effects in Semiconductors (Infosearch, London, 1960) Chapter 4).

19) F.J. Blatt. Solid State Physics Vol. 4, 214-216, 1951.

20) Ref. 19 p.287.

21) C. Herring and E. Vogt. Phys. Rev. 101, 1944, 1956;
105, 1933, 1957.

22) J.M. Ziman. Electrons and Phonons (Oxford, Clarendon P. 1960).

23) G.H. Wannier. Elements of Solid State Theory.
(Cambridge U.P. 1959)

24) H. Jones and C. Zener. Proc. Roy. Soc. A.145, 268, 1934
A.144, 101, 1934

25) W. Shockley Phys. Rev. 79, 191, 1950.

26) R.G. Chambers. Proc. Roy. Soc. A.238, 344, 1957.

27) J.W. McClure. Phys. Rev. 101, 1642, 1956.

28) B. Abeles and S. Meiboom. Phys. Rev. 95, 31, 1954.

29) H.J. Goldsmid. Brit. J. App. Phys. 74, 271, 1963.

30) Ref. 17 p.225.

31) Ref. 16 p.33

32) E.H. Putley. The Hall Effect and Related Phenomena.
(London: Butterworth, 1960).

33) H.J. Goldsmid. Phil. Mag. 8, 1225, 1963)

34) B.S. Chandrasekhar. J. Phys. Chem. Solids 11, 268, 1959.

35) J.J. Mills, R.A. Morant and D.A. Wright. Brit. J. App. Phys.
16, 479, 1965.

36) G.E. Bacon. Acta. Cryst. 4, 558, 1951.

37) P.R. Wallace. Phys. Rev. 71, 622, 1947.

38) W.M. Lomer. Proc. Roy. Soc. (London) A.227, 330, 1955.

39) C.A. Coulson and H. Taylor. Proc. Phys. Soc. (London)
A.65, 815, 1952.

40) J.C. Slonczewski and P.R. Weiss. Phys. Rev. 109, 272, 1958.

41) J.W. Mc.Clure. Phys. Rev. 108, 612, 1957.

42) C.A. Coulson. Valence (Oxford, 1952).

44) F.J. Corbato Proc. 3rd Carbon Conference p.173, 1959.

45) R.R. Haering and S. Mrowzowski. Progress in Semiconductors. Vol. 5. p.273, 1960.

46) D.E. Soule Proc. of 6th Carbon Conference, 1964. p.268.

47) M.S. Dresselhaus and J.G. Mavroides. Proc. of 6th Carbon Conference. 1964, p.262.

48) J.R. Drabble and R. Wolfe. Proc. Phys. Soc. B69, 1956, 1101

49) J.W. Mc.Clure. Phys. Rev. 112, 715, 1958.

50) A.W. Moore, A.R. Ubbelohde and D.A. Young. Proc. Roy. Soc. A.280, 153, 1964.

52) J.W. Harding. Proc. Roy. Soc. (London). A.140, 205, 1933.

53) C.A. Klein. J. App. Phys. 35, 2947, 1964.

54) G.A. Slack. Phys. Rev. 127, 694, 1962.

55) C.F. Gallo, R.C. Miller, P.H. Shutter and R.W. Ure Jr. J.A.P. 33, 3144, 1962.

$$a_\lambda = \frac{1}{\lambda}\left[\frac{5/2+2\lambda}{3/2+2\lambda}\,\frac{F_{3/2+2\lambda}}{F_{1/2+2\lambda}} - \frac{5/2+\lambda}{3/2+\lambda}\,\frac{F_{3/2+\lambda}}{F_{1/2+\lambda}}\right]$$

$$F_p(x) = \int_0^\infty \frac{t^p\,dt}{1+\exp(t-x)}\,,\quad p > -1$$

GRAPH. 1

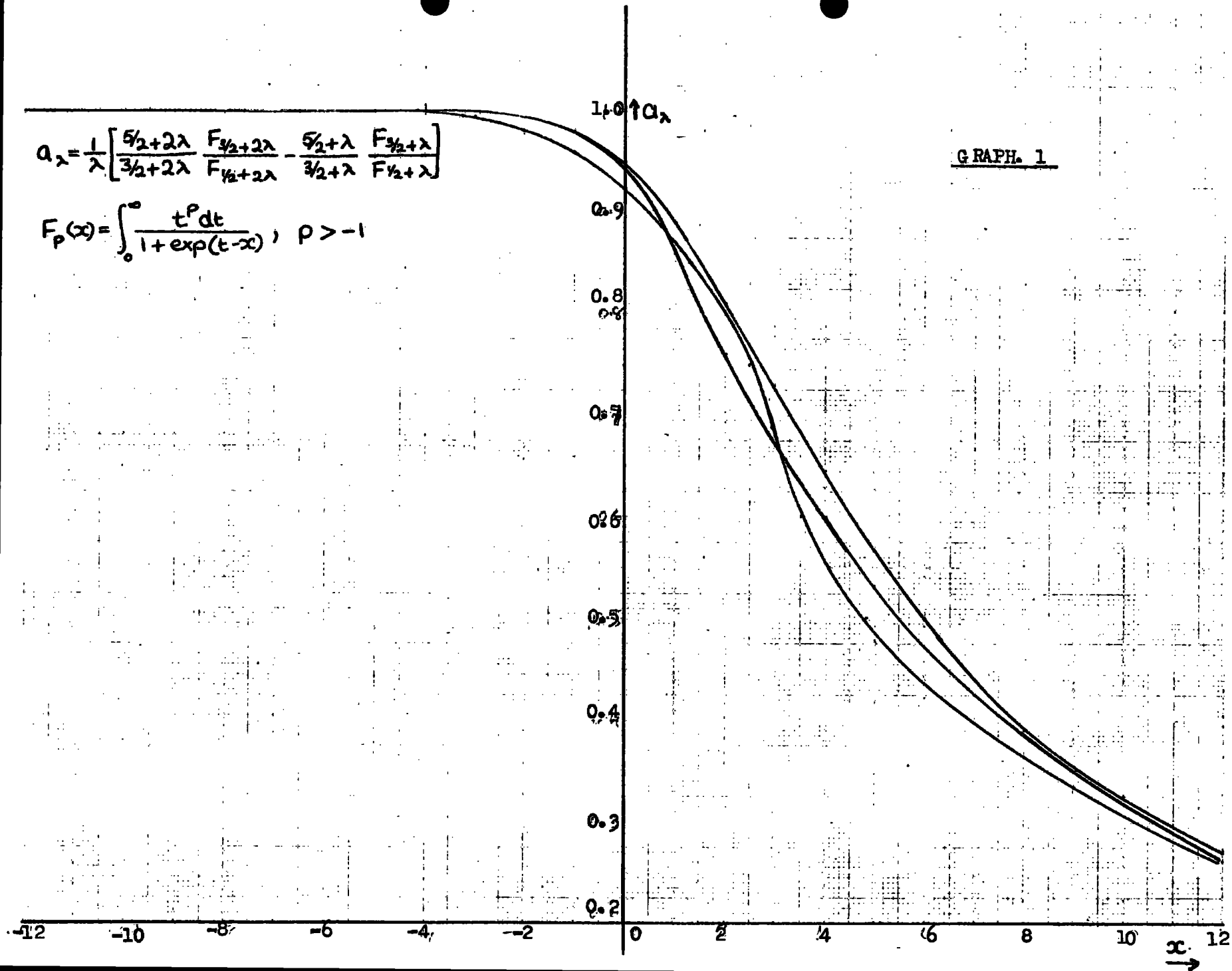

GRAPH 2.

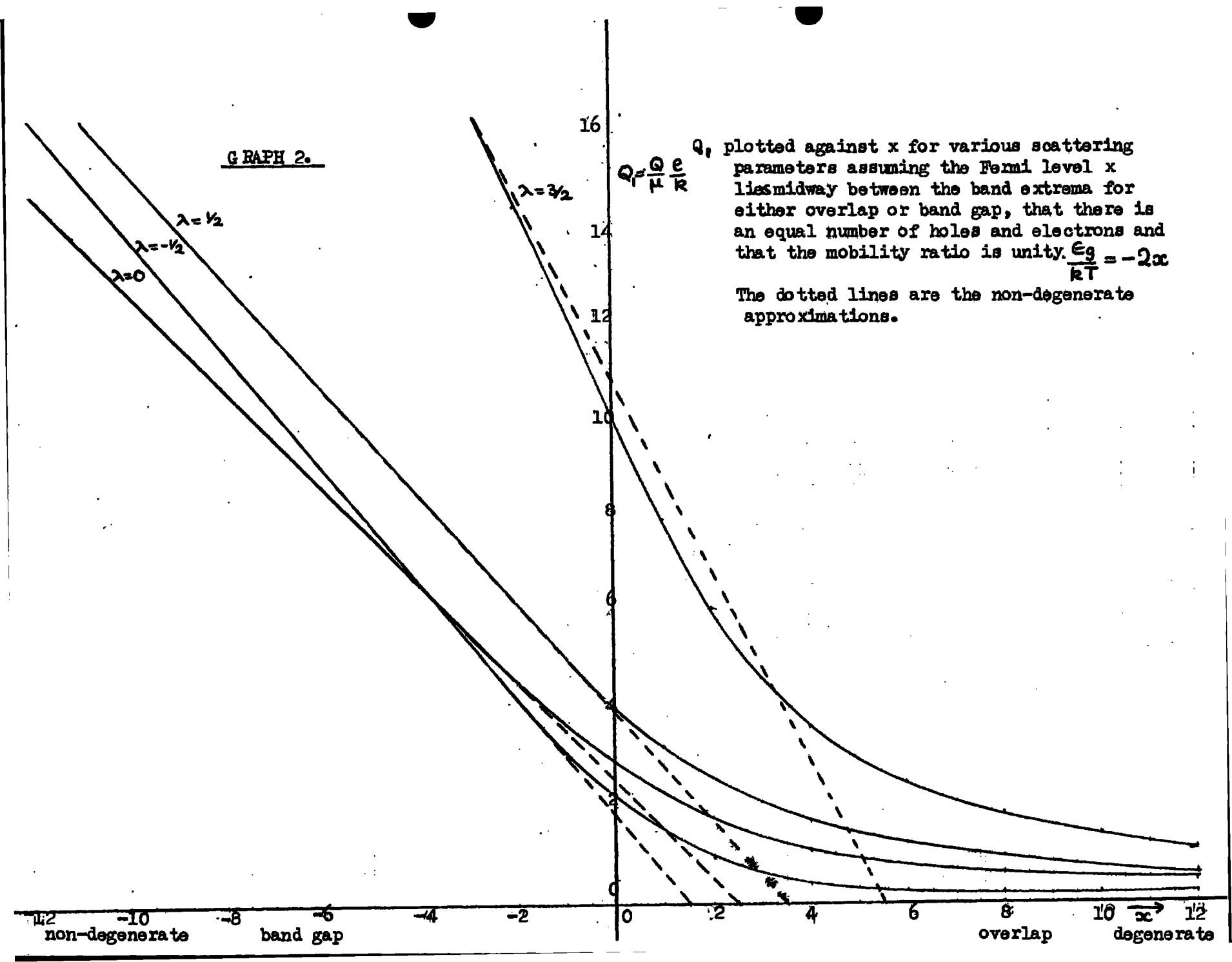

Q_1 plotted against x for various scattering parameters assuming the Fermi level x lies midway between the band extrema for either overlap or band gap, that there is an equal number of holes and electrons and that the mobility ratio is unity. $\frac{\epsilon_g}{kT} = -2x$

The dotted lines are the non-degenerate approximations.

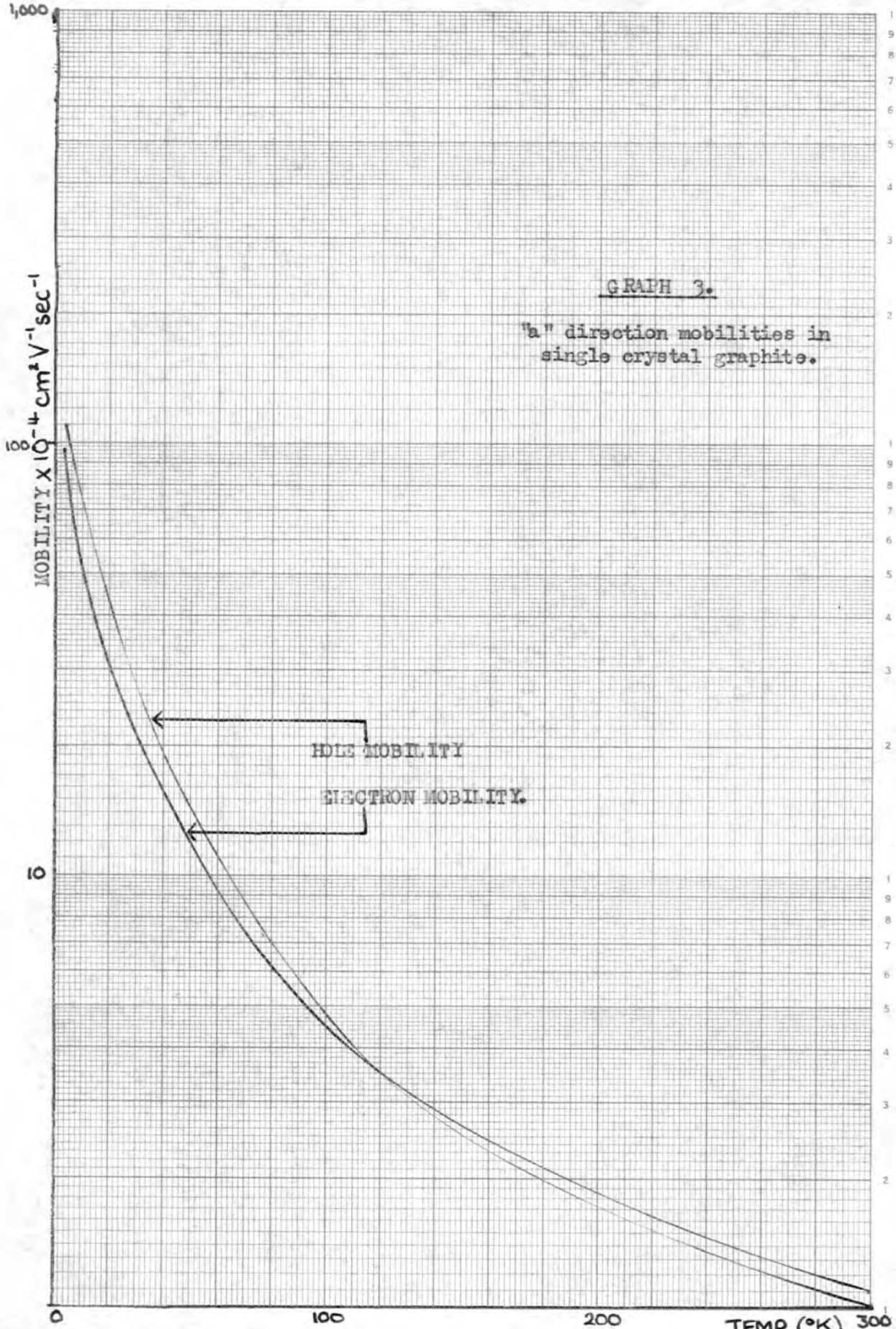

GRAPH 3.

"a" direction mobilities in single crystal graphite.

Q_{12} for acoustic mode scattering ($\lambda = -1/2$)

GRAPH 4.

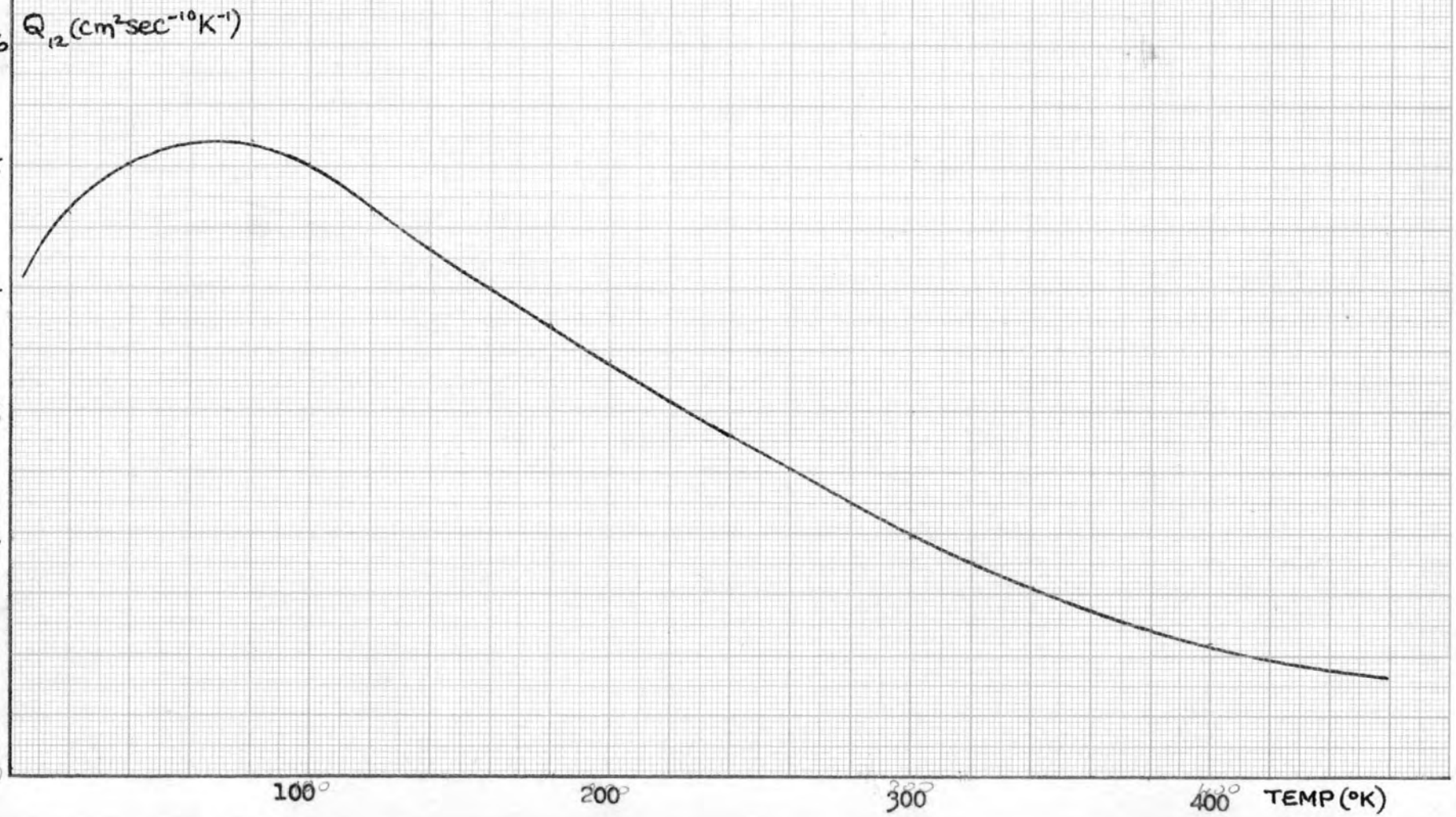

Pure graphite $\epsilon_g = -0.03eV$

$\epsilon_{f_e} = 0.022eV$ = Fermi level for electrons

$\epsilon_{f_h} = 0.008eV$ = Fermi level for holes.

For acoustic mode scattering

$$Q_1 = -\frac{3}{16}\left(a_n P_-^{-1/2} + a_p P_+^{-1/2}\right) + \frac{3}{8}\left(P_-^{-1/2} + P_+^{-1/2}\right)\left[\left\{\frac{F_1(E_{f_e})}{F_0(E_{f_e})} + \frac{F_1(E_{f_h})}{F_0(E_{f_h})}\right\} + \frac{1}{2}\frac{E_g}{kT}\right]$$

$$P_-^{-1/2} = \frac{F_{1/2}(E_{f_e})F_{-1/2}(E_{f_e})}{[F_0(E_{f_e})]^2}\ ;\ P_+^{-1/2} = P_-^{-1/2}(E_{f_h})$$

For boundary scattering.

$$Q_1 = \frac{1}{2}\left[\frac{5}{3}\left\{\frac{F_{3/2}(E_{f_e})}{F_{1/2}(E_{f_e})} + \frac{F_{3/2}(E_{f_h})}{F_{1/2}(E_{f_h})}\right\} + \frac{E_g}{kT}\right]$$

It is assumed that the mobility ratio has a constant value equal to unity and that $\mu B << 1$

$Q_1 = \frac{Q}{\mu}\frac{e}{R}$ GRAPH 5.

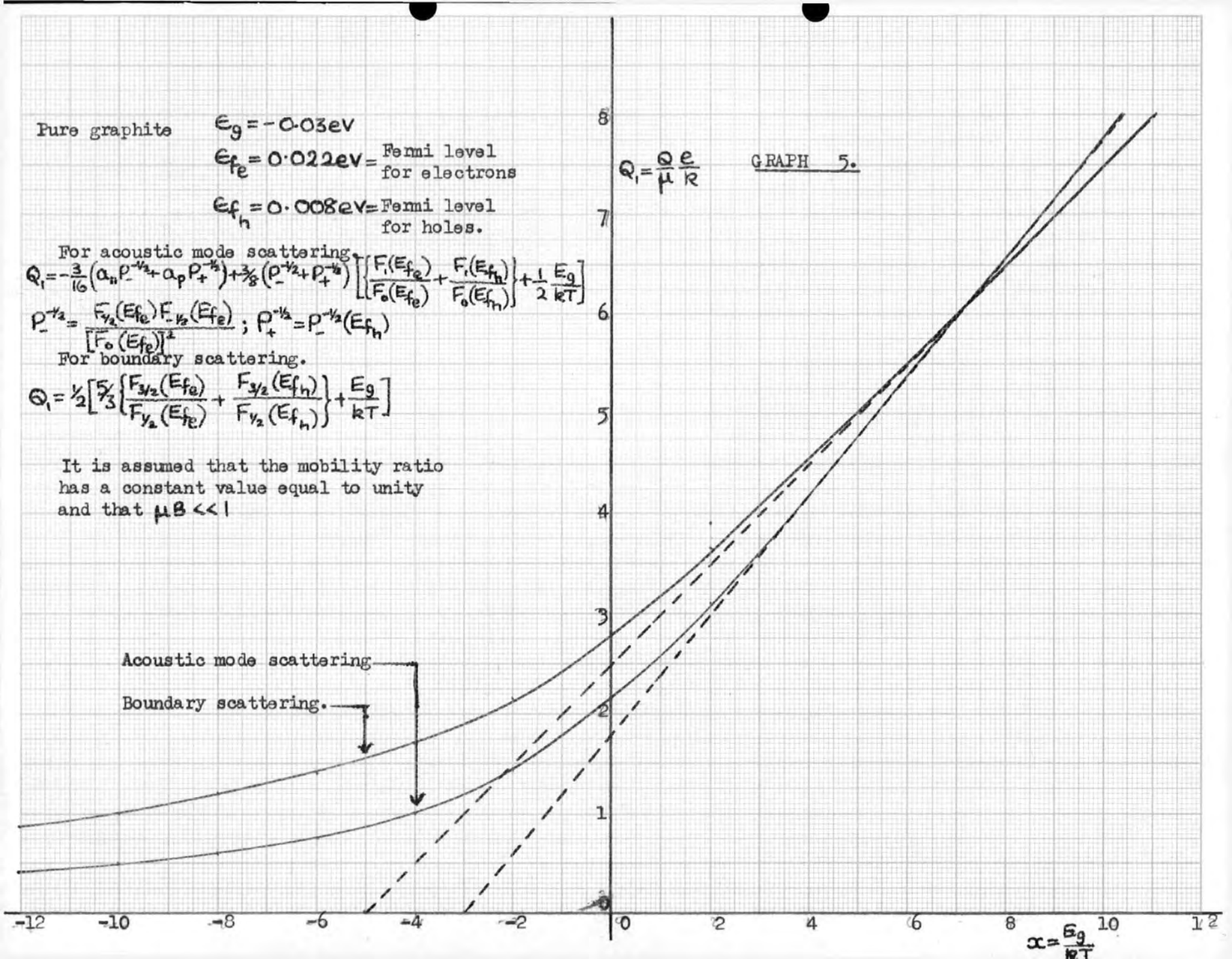

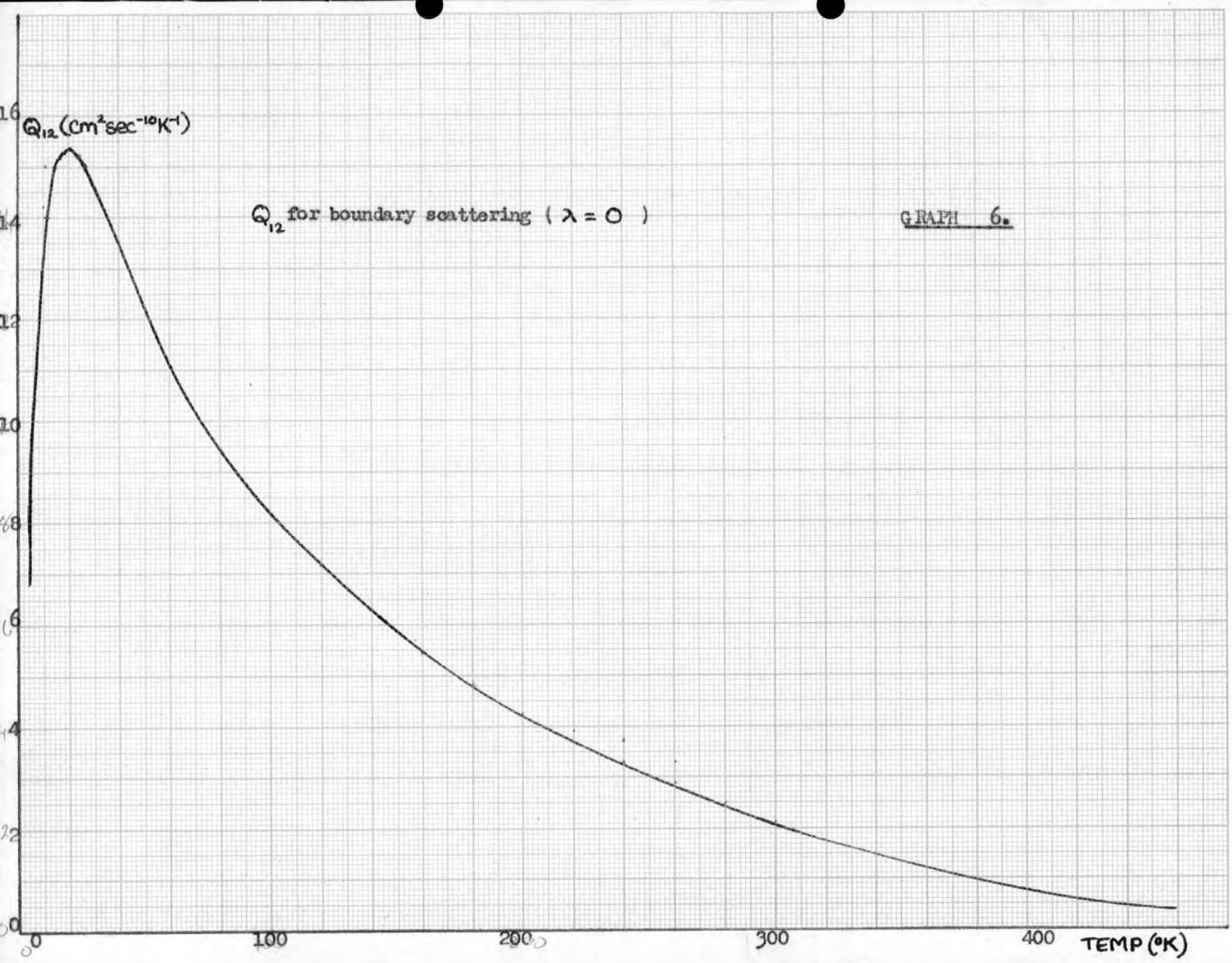

Q_{12} for boundary scattering ($\lambda = 0$)

GRAPH 6.